TALLINN UNIVERSITY OF TECHNOLOGY
SCHOOL OF ENGINEERING

Department of Materials and Environmental Technologies

DEVELOPMENT OF AUTONOMOUS FOOD DEHYDRATION SYSTEM BASED ON BUILDING INTEGRATED PVT TECHNOLOGY

AUTONOOMSE EHITISINTEGREERITUD PÄIKESEPANEELIDEGA TOIDUAINETE KUIVATI PROTOTÜÜP

MASTER THESIS

Student Dmytro Yakobiuk

Student code 156325KAYM

Supervisor Andri Jagomägi, Ph.D., Research Scientist

Tallinn, 2017

AUTHOR'S DECLARATION

Hereby I declare, that I have written this thesis independently.
No academic degree has been applied for based on this material.
All works, major viewpoints and data of the other authors used in this thesis have been referenced.

"....." 2017

Author: .....
/signature /

Thesis is in accordance with terms and requirements

"....." 2017

Supervisor: ….....
/signature/

Accepted for defence

"....."....2017

Chairman of theses defence commission: .....
/name and signature/

TALLINNA TEHNIKAÜLIKOOL
INSENERITEADUSKOND

Materjali ja keskkonnatehnoloogia instituut

AUTONOOMSE EHITISINTEGREERITUD PÄIKESEPANEELIDEGA TOIDUAINETE KUIVATI PROTOTÜÜP

DEVELOPMENT OF AUTONOMOUS FOOD DEHYDRATION SYSTEM BASED ON BUILDING INTEGRATED PVT TECHNOLOGY

MAGISTRITÖÖ

Üliõpilane: Dmytro Yakobiuk

Üliõpilaskood: 156325KAYM

Juhendaja: Andri Jagomägi, Ph.D., Teadur

Tallinn, 2017.a.

AUTORIDEKLARATSIOON

Olen koostanud lõputöö iseseisvalt.
Lõputöö alusel ei ole varem kutse- või teaduskraadi või inseneridiplomit taotletud.Kõik töö koostamisel kasutatud teiste autorite tööd, olulised seisukohad, kirjandusallikatest ja mujalt pärinevad andmed on viidatud.

"....." 2017

Autor: .....
/ allkiri /

Töö vastab bakalaureusetöö/magistritööle esitatud nõuetele

"....." 2017

Juhendaja: .....
/ allkiri /

Kaitsmisele lubatud

"....."..... 2017

Kaitsmiskomisjoni esimees .....
/ nimi ja allkiri /

Table of content

Abbreviations and Acronyms

1-Wire	a serial protocol with a single data line plus a ground reference for communication
BIPV	building integrated photovoltaic
BIPVT	building integrated photovoltaic thermal
HRU	the heat recovery unit
HS	humidity sensor
I^2C	a serial protocol for two-wire interface to connect low-speed devices like microcontrollers and other peripherals in embedded systems
MOSFET	metal-oxide-semiconductor field-effect transistor
PV	photovoltaic
PVT	photovoltaic thermal
PWM	pulse width modulation
Ref.	reference
TS	temperature sensor

Symbols

Symbol	Description (value)	Units
A	area	m^2
c_{ps}	specific heat capacity of Polystyrene (1300)	J/kg °C
c_{pw}	specific heat capacity of oriented strand board (1210)	
c_{ms}	specific heat capacity of metal sheet (465)	
c_{pol}	specific heat capacity of polyolefin (2400)	
c_c	specific heat capacity of cells (710)	
c_{gl}	specific heat capacity of glass (767)	
CV	convective heat transfer	W/m^2
CD	conductive heat flow	W/m^2
D_h	air channel hydraulic diameter	m
d	the thickness of the air channel (0.05)	m
G	radiation intensity	W/m^2
h	convective heat exchange rate	$W \cdot m^{-2} \cdot K^{-1}$
I	current	A
IR	infrared heat flow	W/m^2
k_{ps}	thermal conductivity of Polystyrene (0.2)	$W \cdot m^{-1} \cdot K^{-1}$
k_{pw}	thermal conductivity of oriented strand board (0.12)	
k_{ms}	thermal conductivity of metal sheet (54)	
k_{pol}	thermal conductivity of polyolefin (0,28)	
k_c	thermal conductivity of cells (148)	
k_{gl}	thermal conductivity of glass (1)	
m	mass	kg
$\dot{m}$	mass flow rate of the air	kg/s
$NOCT$	nominal operating cell temperature	°C
P	power	W
T	temperature	°C
U	voltage	V
VF_{sky}	sky view factor	
VF_{gr}	ground view factor	
v_{air}	air flow speed	m/s
x_{ps}	layer thickness polystyrene (0,03)	m
x_{pw}	layer thickness oriented strand board (0,015)	
x_{ms}	layer thickness metal sheet (0,6)	
x_{pol}	layer thickness polyolefin (0,0045)	
x_c	layer thickness cells (0,0018)	
x_{gl}	layer thickness glass (0,02)	
α_{PV}	absorption of cells (0,97)	
α_{gl}	absorption of glass (0,01)	
σ	Stefan-Boltzmann constant ($\sigma = 5.670367(13) \times 10^{-8}$)	$W \cdot m^{-2} \cdot K^{-4}$
ϵ_{gl}	emissivity of glass (0.84)	
ϵ_{ms}	emissivity of metal sheet (0,84)	
ϵ_{pl}	emissivity of oriented strand board (0,84)	
η	efficiency	%
ρ_{ps}	density of Polystyrene (1345)	kg/m^3
ρ_{pw}	density of oriented strand board (540)	
ρ_{ms}	density of metal sheet (7900)	
ρ_{pol}	density of polyolefin (950)	
ρ_c	density of cells (2330)	
ρ_{gl}	density of glass (2450)	
τ_{gl}	transmittance of glass (0,93)	
γ	power coefficient of solar panel	

1. Introduction

Food dehydration industry is very popular sort of food preservation all over the world. One competitive food drying technology is indirect solar drying and *Figure 1* shows the reasons to use this technology. The first reason is that traditional food dehydration industry consumes a large amount of energy that mainly comes from fossil sources. Due to the negative impact on the environment and high prices of fossil fuels, there is a drive to seek for alternatives. Another advantage of solar drying is the use of free abundant primary energy source. Thus, there is no need to pay for energy. It is well-known fact that open solar drying of the agricultural products for preservation existed for thousands of years. However, this process is far from ideal and does not meet the international requirements. Rodents, birds, insects, dust or weather conditions could easily affect the product quality. To prevent this, people used direct solar dryers with protective envelope and glass cover. However, both direct and open solar dryers expose the product to the direct solar rays. The ultraviolet radiation causes the discoloration of the product [1]. In addition, it is very difficult to control the drying rate and if it is too high the commodities could be overly dried. On the other hand, if the sun is not available the drying rate could be too low. Thus, the product could not be dry in time and could be spoiled. That is why for this purpose it is reasonable to use other methods of solar radiation conversion such as a use of the thermal collectors. It should be noted, that in the northern latitudes there is a very good temporal match between the vegetation period and the availability of solar irradiation. This fact makes solar drying even more attractive.

When the crop is ready, it is essential to provide suitable temperature regime and the continuous process of food dehydration even in the night. Drying systems must usually run 24/7. Thus, the challenge in solar drying is how to deal with the volatility of irradiance level. Also sometimes, it is reasonable to dry products at the places of the harvest, because dried products are easier to transport and store. However, the problems may occur with the access to the electric grid in the fields. Therefore, it is reasonable to develop a portable and energetically autonomous food dehydration system. A use of BIPVT hybrid collectors as electric and a heat source is considered as a promising technology for this application. Since such collectors increase the efficiency of the solar cells, allow extracting waste heat and serve as parts of drying cabinet, thus decreasing construction cost.

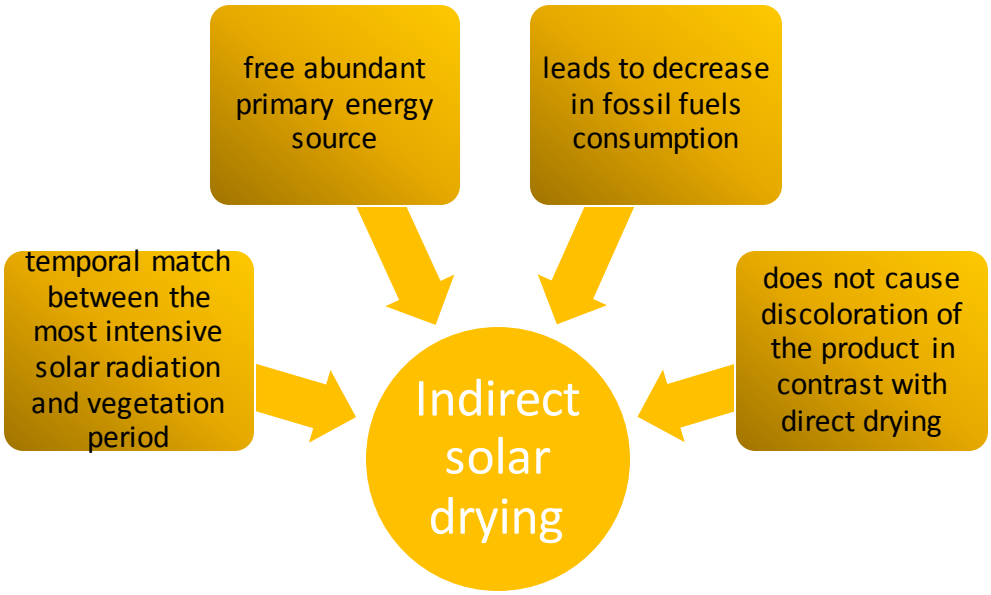

Figure 1. Reasons to use indirect solar dehydration

The aim of the study is to share experience in designing, building and testing of the portable and energetically autonomous food dehydration system with HRU based on the air type BIPVT roof; to perform simulations of drying system performance under different climate conditions (Tallinn, Estonia and Provence, France) in order to estimate feasibility of this technology.

2. Literature review

2.1. Review of PVT technology

Currently, most popular technologies utilize the solar energy for the conversion into the electricity and the heat separately. However, there has been growing interest in the PVT technology over the last decades Refs. [2], [3], [4], [5], [6]. The great potential of this technology has been recognized in 1970th [7]. The main advantages of the PVT system are [8]:

1. The system produces the electric power and the heat energy simultaneously as it shown on Figure 2.

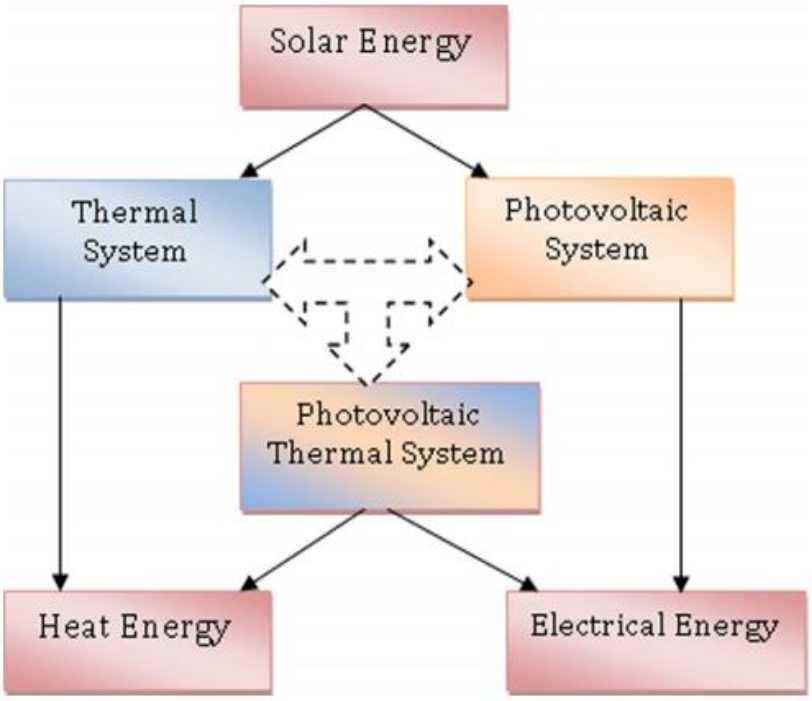

Figure 2. The schematics of the different conversion systems of the solar energy *[8]*

2. It is efficient to use the hybrid PVT system, as efficiency is always higher in comparison with the use of two separate systems photovoltaic and thermal.

3. The system is particularly attractive for an application of the building integrated photovoltaic (BIPV) systems where the roof area is limited.

4. It is cost effective and practical. The system is easy to integrate into buildings' envelope without any major modification and requires less space and materials. PVT system has the shorter payback period comparing to separate PV and thermal systems.

The PVT air collectors are simply flat plate solar air heaters with photovoltaic cells placed on the absorber plate. Figure 3 presents the main types of widely used PVT collectors.

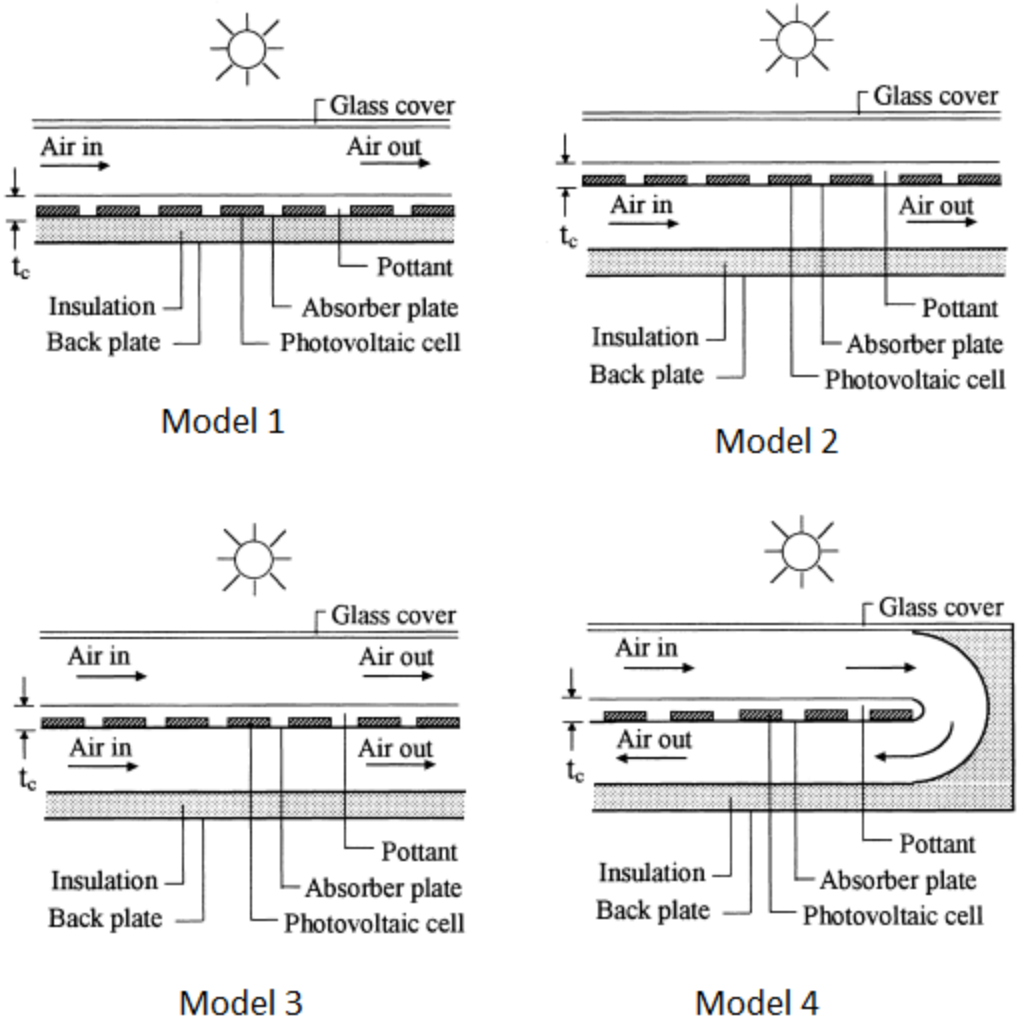

Figure 3. Widely used configurations of PVT collectors *[9]*

Paper in Ref. [9] investigates the performances of four widely used configurations of PV/T air collector shown on Figure 3. The first Model represents the PVT collectors where the air duct is organized above PV module. In the second Model, the air duct is under the PV module and additional glazing presented above. The third Model has two air ducts for running the air under and above the PV module. And the fourth has two channels for the double pass of the air above and then under the PV module. Results showed that the rating of the models starting from the highest has the following order: third, fourth, second and first. In addition, it has been shown that each of these models has a critical air mass flow rate beyond which the

performance decreases. It should be noted that the structure of such collectors are rather complex for the use of the building integration and the cost is high.

Solanki et al. have designed and manufactured the hybrid PVT collector for studying of its performance under indoor conditions [10]. Figure 4 shows the gain of the electrical efficiency by the use of the PVT technology in comparison with the PV technology. On the graph, two curves reflect the efficiency and the temperature of the cell in the PVT module with air flow and the other two the efficiency and the temperature of the cell in the ordinary PV module. The efficiency of the cooled cell is higher.

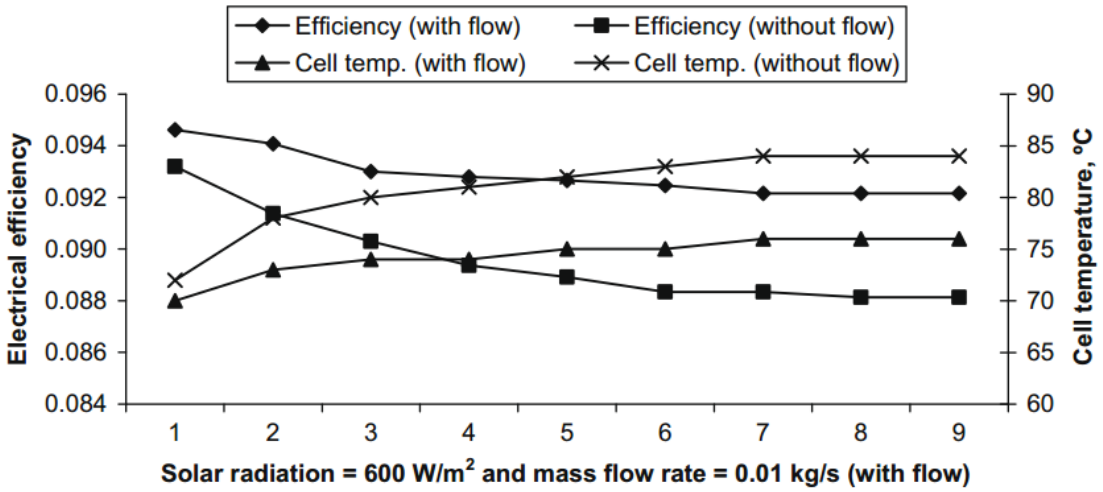

Figure 4. The electrical efficiency and cell temperature in case of with and without air flow in the channel *[10]*

Figure 5 shows thermal, electrical and overall efficiencies of the PVT collector versus flow rate. The thermal and electrical efficiencies of the hybrid solar collector are 42% and 8.4%, respectively. The overall efficiency it about 50% which is much higher than the efficiency of PV module. Authors emphasized the importance of the use of the PVT technology over PV as it increases the electric efficiency and allows producing the heat energy.

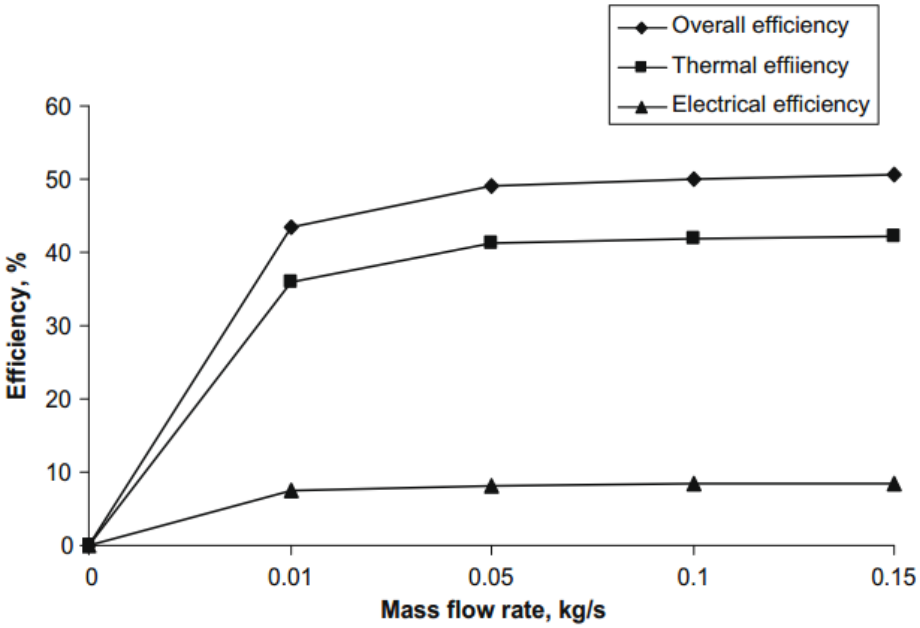

Figure 5. Effect of mass flow rate on thermal, electrical and overall efficiency at solar radiation 600 W/m2 and inlet air temperature into PVT collector 38 °C *[10]*

Agrawal et al. have conducted performance analysis and life cycle cost estimation of the BIPVT systems with various PV modules based on mono-crystalline Silicon, poly-crystalline Silicon, ribbon crystalline Silicon, amorphous Silicon, Cadmium Telluride and Copper Indium Gallium Selenide solar cells in the Ref. [11]. The authors have provided the comparison with the analogical BIPV system. It has been shown that in all cases it is beneficial to use BIPVT technology rather than BIPV in terms of the energy efficiency and the cost effectiveness.

Consequently, according to previous scientific papers, it is reasonable to use hybrid BIPVT collectors as heat and power source for autonomous and portable food dehydrators rather than thermal collectors and PV modules separately.

2.2. Indirect solar dryers so far

According to Ref. [12], indirect solar dryers with forced air movement comprises the following main elements: solar collectors, dehydration chamber, auxiliary heater and fan in most cases. Ruslan et al. in the study in Ref. [13] presented portable indirect solar dryer with the thermal collector, PV panel and fan. The thermal collector was based on the V-grooved metal sheet and served as the heat source. In this system PV panel supplied electricity for the fan. According to the report, during a day they have achieved the average efficiency and the

temperature in the drying chamber of 44 % and 46 °C respectively with the average flow rate and the average solar irradiation of 0.16 kg/s and 800 W/m^2 respectively. Thus, they have demonstrated a big potential of PV assisted indirect solar drying.

An auxiliary source of heat is very important in solar drying systems, as solar radiation is an intermittent source of energy. Previous studies investigated numerous options of auxiliary heat sources such as an electrical heater presented in Refs. [14], [15], heat pump, biomass and LNG burners presented in Ref. [12] etc. The experimental research of indirect solar dryers in Ref. [15] based on V-groove steel sheet collectors with the electrical heater and without showed that the drying time of the products is significantly reduced with using the heater by 4-6 hours and efficiency is increased by 25%.

Several studies in Refs. [16], [17] investigated indirect solar dryers with PVT collectors as an energy source. In Ref. [16] authors have presented a double pass PVT solar air collector with compound parabolic concentrator and fins for using in solar drying. In this investigation, authors conclude that the system showed satisfactory performance and it is suitable for usage in rural without an electrical grid. Another theoretical work in Ref. [17] conducted the energetic analysis of double pass PVT hybrid panels in an indirect solar drying application and proved that such a system produces higher temperatures for dehydration process.

In previous scholars, research have tended to focus on an investigation of the solar thermal in Refs. [13], [15] and double pass PVT collectors in Refs. [16], [17], rather than on BIPVT hybrid collectors. Apart from the fact that latter produce electricity and heat energy simultaneously, it replaces a traditional roof or building envelope and therefore reduces the construction cost. In return, double pass collectors have higher efficiency [12], [16] in comparison with single pass collectors. However, they have complicated structure and high cost.

McDoom et al. proposed usage of PV system with batteries for running blower in Ref. [18]. Authors report that PV system could supply blower with the electricity for two weeks and the batteries could provide the electricity for the fan for 2 days during low solar radiation. However, a little attention was dedicated to the use of PV panels system with batteries as an energy source for supplying electricity to the drying system's elements such as a heater and controlling system when there is no solar radiation or in the night.

Aktas et al. investigated solar-heat recovery assisted infrared dryer in Ref. [19]. The authors have shown that infrared drying had much better performance with the contribution of the solar energy and heat recovery rather than single infrared drying. Paper claims that heat recovery unit increases overall performance by 23 – 28%.

According to previous studies concerning of indirect solar dryers, it is reasonable to use an auxiliary heat source, battery to store electricity and provide continuous drying process and a heat recovery unit to increase an overall efficiency of the system. A little attention was dedicated to providing of energy autonomy of the system, suitable temperature regime in drying chamber and continuous drying process even in the night.

3. Description of the setup

3.1. Description of the cabinet

BIPVT collectors-based solar drying system is a small portable cabinet with the roof area of 7 m^2 and the photos are shown on Figure 6 and Figure 7. For convenient transportation, the cabinet is mounted on the wheels.

Figure 6. The test bench of food dehydrator (view from the back)

Figure 7. The test bench of food dehydrator (view from the front)

Figure 8 and Figure 9 present 3D model of the system. There are the drying chamber, fan, heater, heat recovery unit (HRU) and the piping system inside the cabinet. In addition, the system is equipped with the batteries, the charge controller, and a number of temperature and humidity sensors to monitor the system performance. To monitor the drying process online, the drying chamber is mounted on four load cells. Based on the microcontroller ATmega2560, the Arduino Mega board monitors and controls the whole system as well as logs the data in the web server.

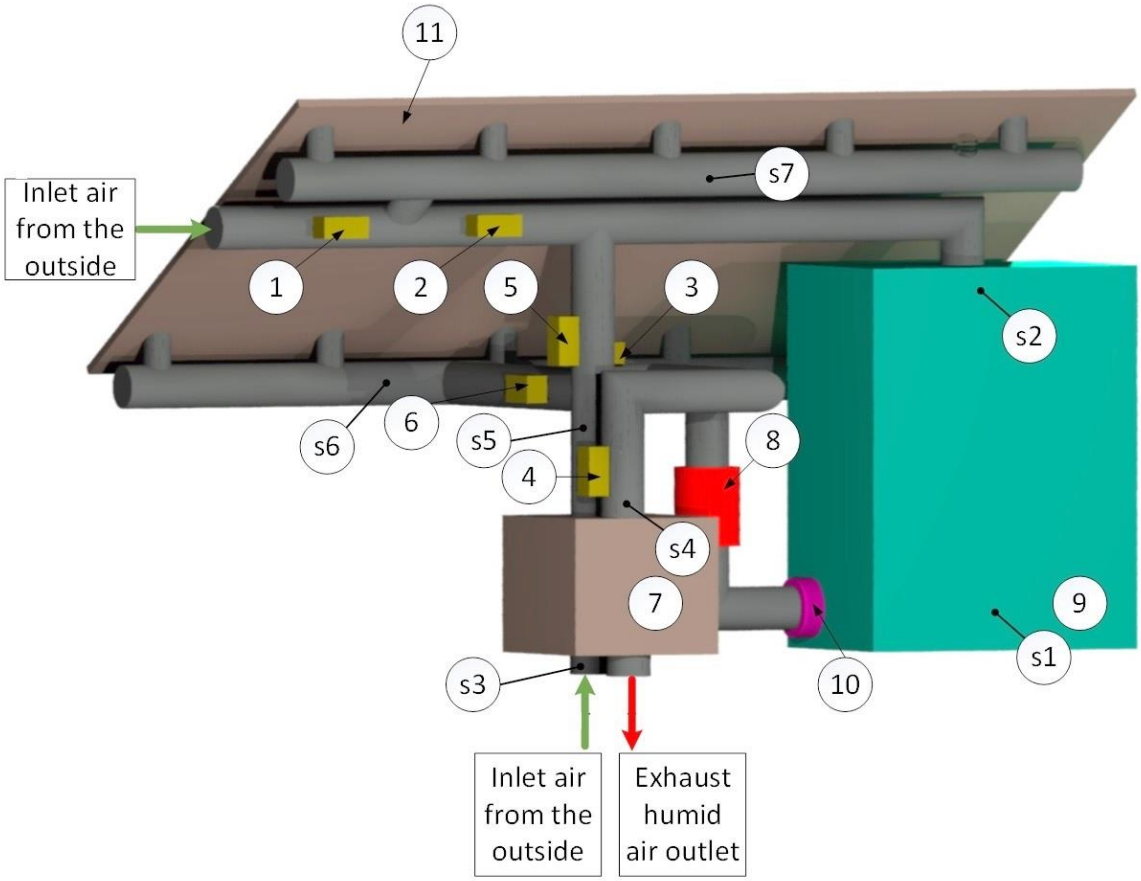

Figure 8. 3D model of autonomous food dehydrator test bench (view from the back):

1-6 – dampers; 7 – HRU; 8 – heater; 9 – dehydration chamber; 10 – fan; 11 – photovoltaic thermal channel; s1, s2 – temperature (TS) and humidity (HS) sensors on the top and on the bottom of drying chamber respectively; s3 – temperature sensor for cold inlet air into HRU; s4 – TS for hot outlet air into HRU; s5 - TS for hot inlet air into HRU; s6 - TS for cold inlet air into BIPVT collectors; s7 - TS for hot outlet air from BIPVT collectors.

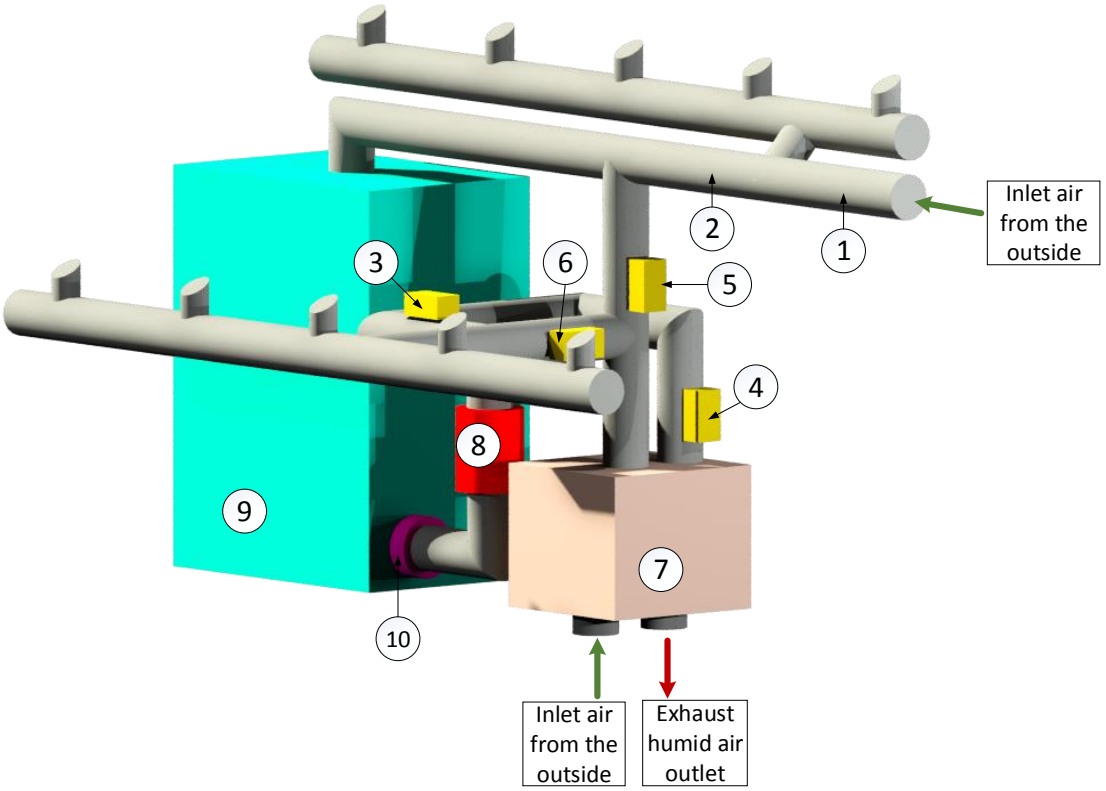

Figure 9. 3D model of autonomous food dehydrator test bench without BIPVT collectors (view from the front): 1-6 – dampers; 7 – HRU; 8 – heater; 9 – dehydration chamber; 10 – fan; 11 – BIPVT collectors; s9 - TS on the top of BIPVT collector; s8 - TS on the bottom of BIPVT collector.

The drying chamber is actually a rectangular box with a height, depth and width of 1.2, 0.6, 1 m respectively. The walls of the chamber are built using the oriented strand boards, which is insulated using polystyrene from the outside in order to reduce the heat losses. The air flows from the bottom to the top of the chamber. Therefore, the trays are made of wooden frames and stainless steel wire mesh that allows air to move through them freely. The maximum possible number of trays in the chamber is 10. Dimensions of the trays are 1 m by 0.6 m. The distance between the trays' levels is 0.1 m. The pipes with the diameter of 16 and 10 cm carry the pipelines between the different elements of the system.

3.2. Description of PVT collectors

The roof cover is made of standing seam metal sheet integrated photovoltaic modules. The total rated power of the modules is 1 kW. Figure 10 shows the structure of the BIPVT collectors. Metal sheet integrated photovoltaic modules consist of glass, metal sheet and photovoltaic cells laminated between using polyolefin (1-4).

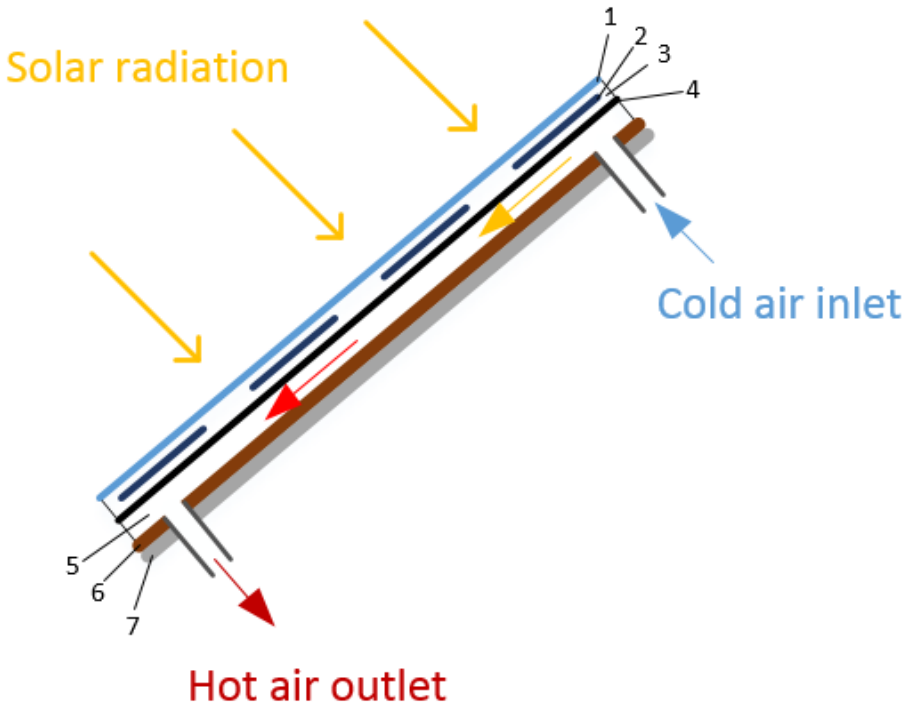

Figure 10. Schematic diagram of BIPVT collector's structure: 1 – glass; 2 – photovoltaic cells; 3 – layer of polyolefin; 4 – black metal sheet; 5 – air gap; 6 – oriented strand board; 7 – polystyrene

When the modules absorb solar radiation, photovoltaic cells convert part of radiation into electricity and other part heats the modules. This waste heat is extracted by the following method. Behind the modules, there is an air channel (5) that is used to run the air by the fan and, thus, heat it. The channel was built using oriented strand board (6) and polystyrene (7) for insulation. The dimensions of PVT channel in a single collector are 0.005x0.7x2m. There are five of such collectors. They were optimized using the thermal simulation model [20].

3.3. Power management

The PV modules produce the electrical energy to power the heater, fan, and the electronics. The surplus of electrical energy produced during the daytime is stored in the batteries and used to power all the elements when the solar radiation is unavailable or in the night. There are two batteries with the electrical capacity of 100 Ah and voltage of 12 V that are connected in parallel. Figure 11 shows the power supply to all the elements of the system.

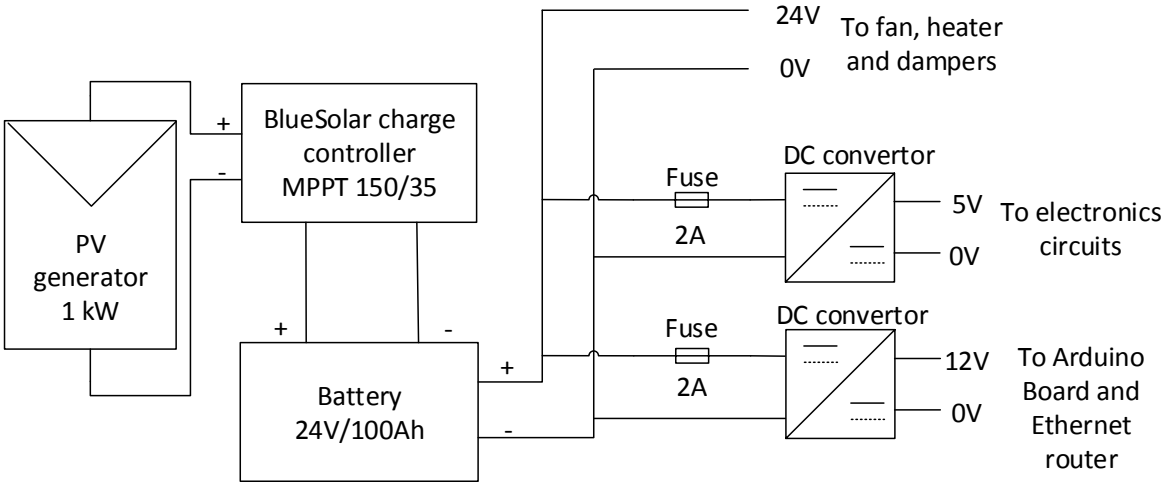

Figure 11. Power supply schematics of the system

3.4. Operational modes

The system runs in three operational modes. The operational modes are set by changing the positions of the dampers. The dampers control the air path through the system. ide *suitable* temperature regime.

Table *1* presents the dampers' positions, fan's and heater's states for different modes. It should be noted that the fan's speed is used to control the temperature regimes inside the drying chamber in all the modes 1 and 2. In order to save electrical energy in Mode 3, the heater works on the minimum power needed to provide suitable temperature regime.

Table 1. The matrix of the dampers' positions, fan's and heater's states

Mode	**Dampers (1 – opened, 0 – closed)**						**Heater**	**Fan**
	#1	#2	#3	#4	#5	#6		
1	1	0	1	0	1	0	off	on
2	0	1	0	1	0	1	on	on
3	0	0	0	1	1	0	on	min

Figure 12 shows schematically how the air passes through the system in the Mode 1. The fresh air is taken directly from outside, heated in the PVT channel and directed to the drying chamber. Mode 1 is designed for the periods with the most intensive solar radiation when the heat production from BIPVT modules is high enough to provide suitable temperature regime in drying chamber. The temperature in this mode is controlled by the fan speed. If the actual

temperature gets higher than set point temperature, program increase the fan speed and therefore air flow rate.

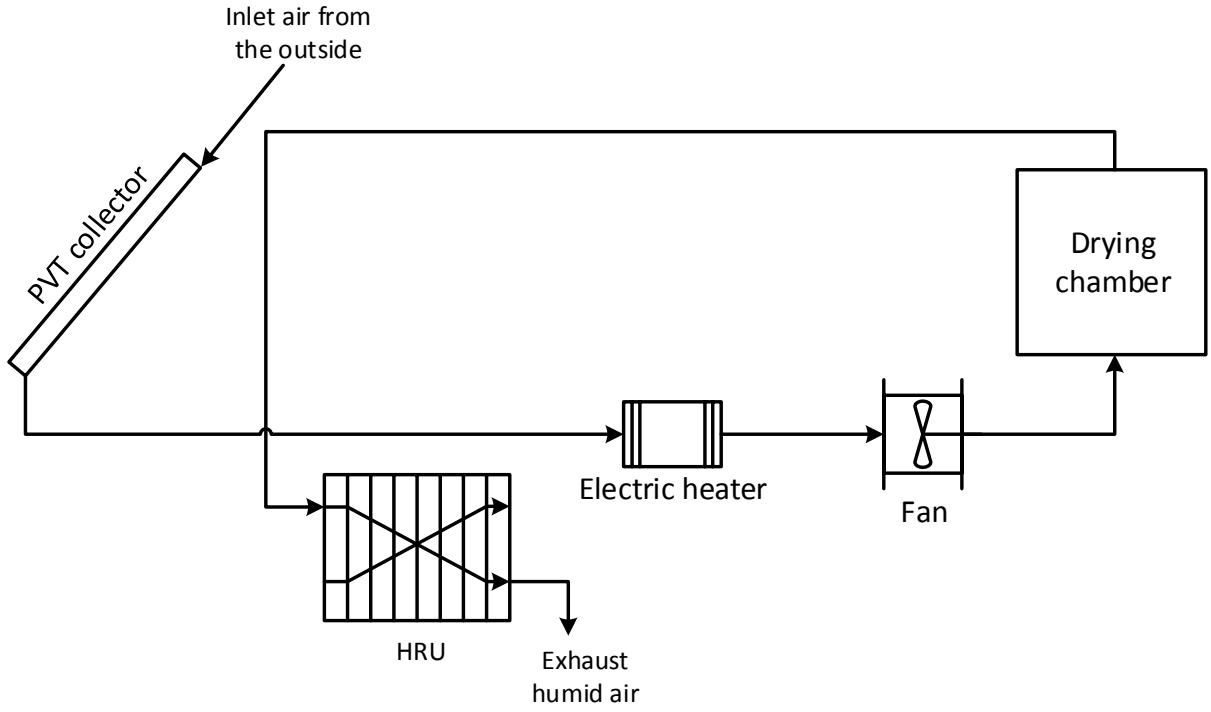

Figure 12. Schematic representation of air flow through the system in Mode 1

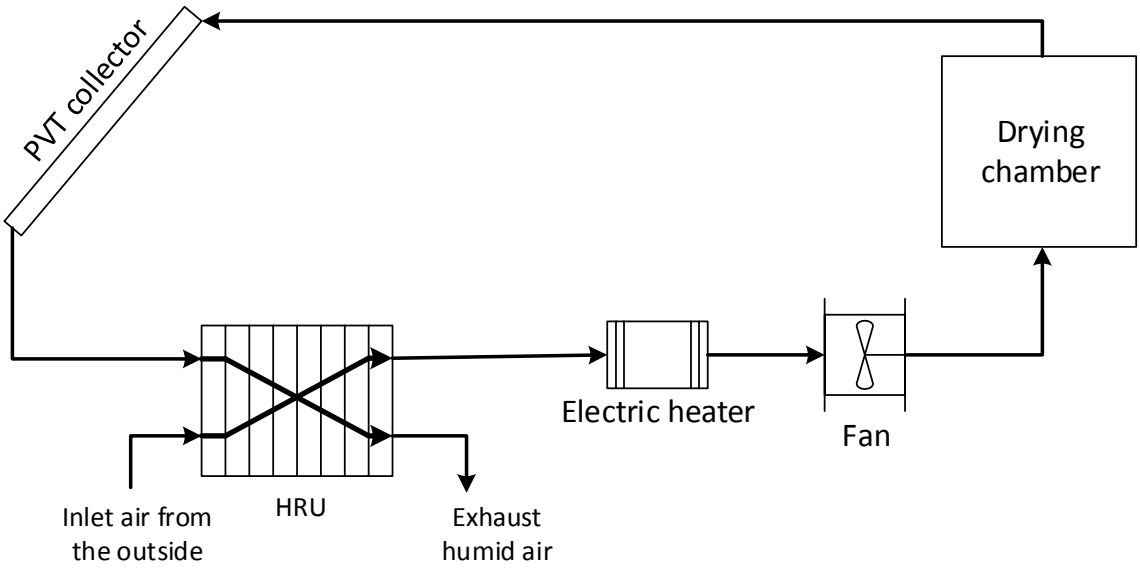

Figure 13. Schematic representation of air flow through the system in Mode 2

In Mode 2 the fresh air is preheated in HRU by exhaust air and if it is not high enough heated by the electrical heater and then by the PVT channel. Figure 13 presents the scheme of

the air path through the system in Mode 2. This Mode is intermediate between Mode 1 and 3 and designed for low-level solar radiation periods. The temperature is regulated by the fan speed and heating power in this case.

Figure 14 presents the scheme of the air path through the system in Mode 3. In Mode 3, the air is heated by the electrical heater. In addition, the HRU is used for the heat recovery. This mode is designed for nighttime or when the solar radiation is unavailable. In this mode, we decided to bypass PVT collectors as the temperature of the outside air in the night could be quite low in Estonian conditions. Therefore, the air would rather cool down in PVT channel.

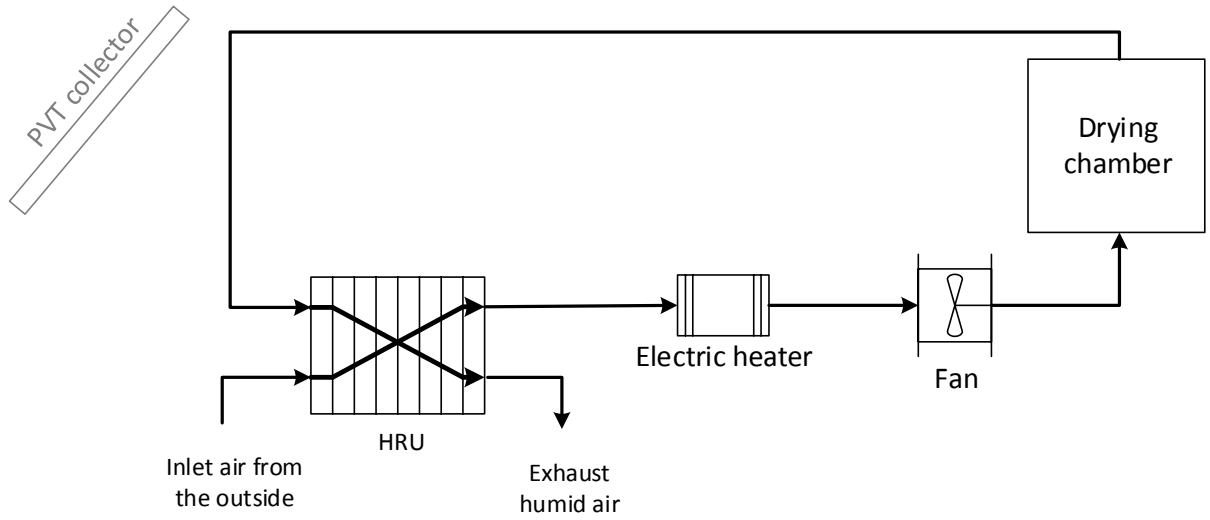

Figure 14. Schematic representation of air flow through the system in Mode 3

3.5. Electronic circuits for controlling the system's elements

Arduino's digital pins control the positions of the dampers by sending a digital signal to the relay of the corresponding damper's actuator. Digital pin 3 controls the dampers 1 and 3, digital pin 4 controls the dampers 2 and 6 and digital pins 5 and 2 control dampers 5 and 4 respectively. Figure 15 shows the typical electronic circuit for single damper control.

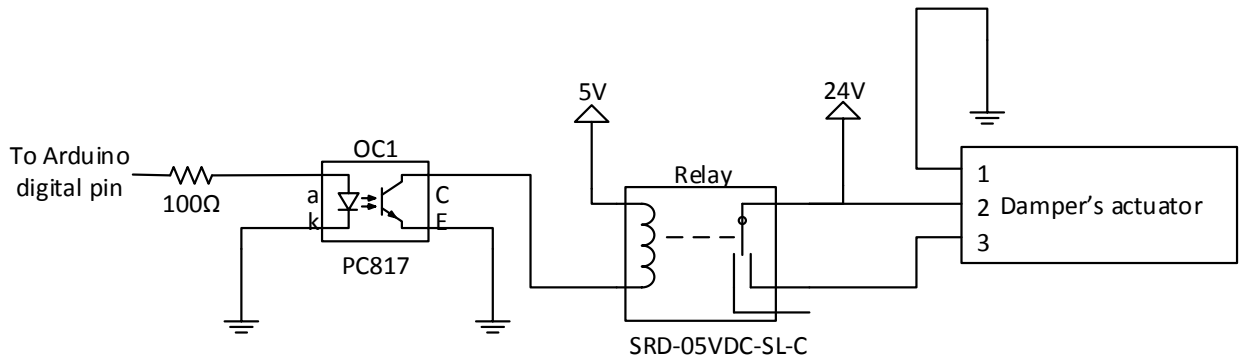

Figure 15. The schematics of the typical electronic circuit for the damper control

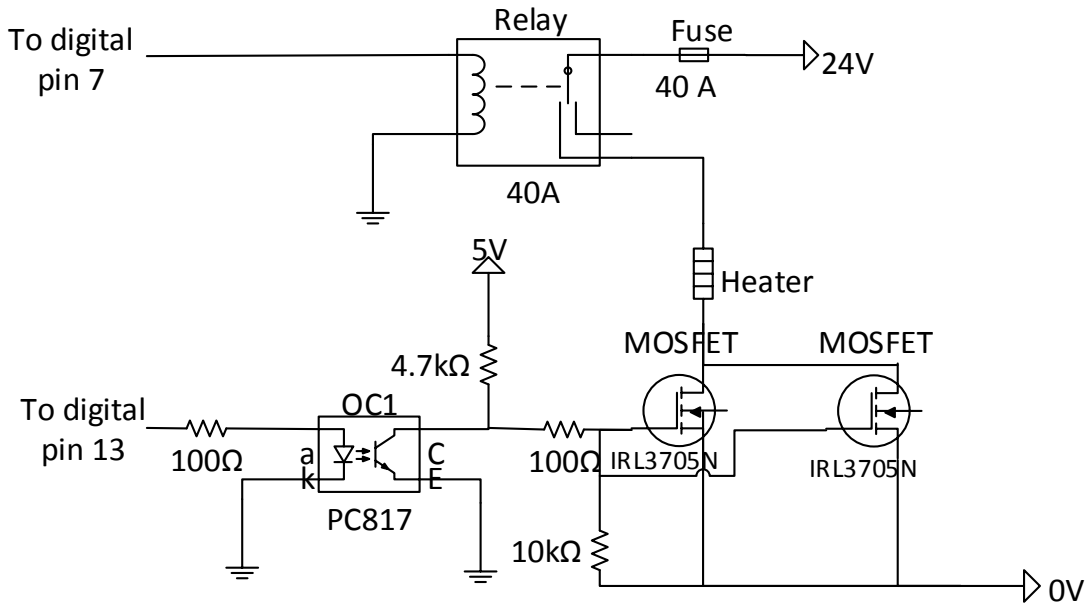

Figure 16. The schematics of the electronic circuit for the heater's control

The heater's power is controlled by pulse width modulation (PWM). Figure 16 presents the schematics of the electronic circuit for controlling the heater's power. PWM signal from Arduino's digital pin 13 to the gate of the MOSFET allows controlling the effective voltage on heater's clamps. Since the rated current of the heater is 16.6A the work of two MOSFETs was organized in parallel in order to reduce the load on the single MOSFET. The relay was added due to the safety issues and is controlled by the digital pin 7.

Two Arduino's digital pins control the fan. Digital pin number 9 generates a PWM signal with changeable duty cycles, thus controls the fan's speed. Pin 6 controls safety relay. The fan has a built-in tachometer and digital pin 8 performs readings of the tachometer. Figure 17 shows the electronic circuit diagram for controlling of the fan.

The connection of the temperature and humidity sensors is organized in parallel and coupled with the 1-Wire slave to I^2C master bridge device (DS28E17). Figure 8 and Figure 9 show the detailed position of the temperature and humidity sensors. Four load cells YZC-516 were used to measure the products weight in the drying chamber. They have the parallel connection to the load cell amplifier (HX711). In addition, batteries voltage measurements were organized with a simple voltage divider.

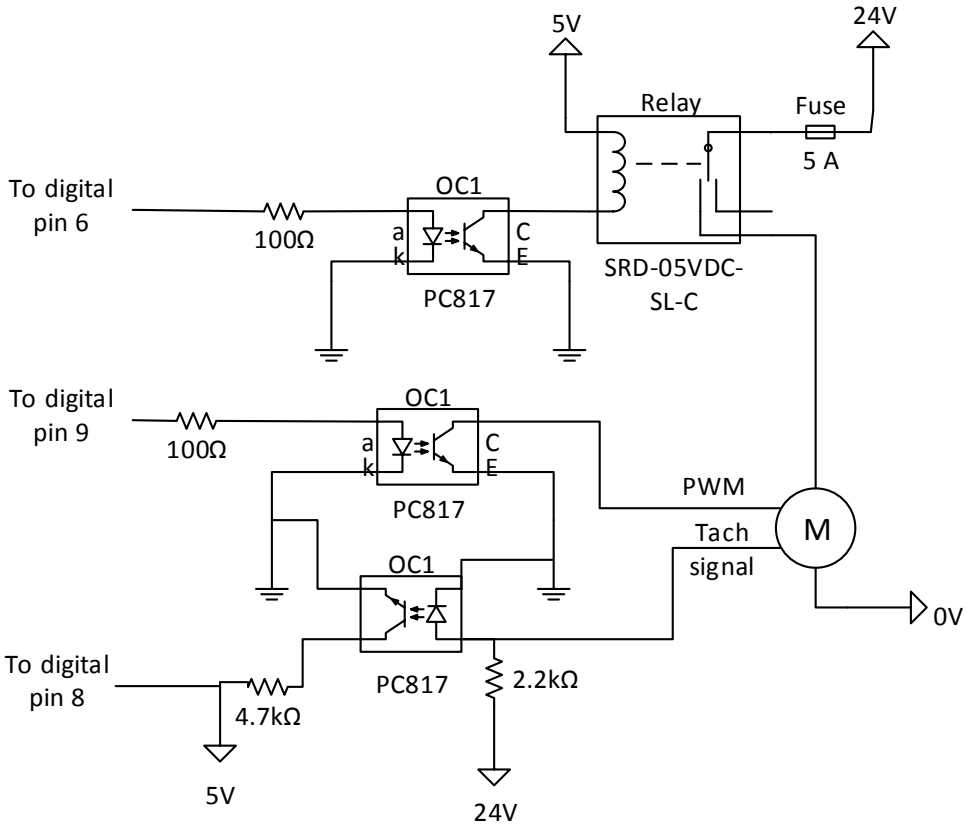

Figure 17. The schematics of the electronic circuit for the fan's controlling

3.6. Software

The software for the microcontroller was implemented in C++ programing language. The program consists of two main subroutines Setup Function and Loop Function. Once the microcontroller is switched on, Setup Function executes initialization. Figure 18 shows the flowchart of possible Setup Function. The latter also defines the initial operational mode based on the temperature of PVT modules (T_9) and inlet air temperature (T_3). If the temperature of PVT modules is higher, it means that there is solar radiation and Mode 2 to be chosen. If it is not higher, Mode 3 is chosen.

Figure 19 presents possible Loop Function flowchart. This part of the program is executed in the endless loop. Generally, each period of time ($\partial\tau$) it takes T_{sp} value from the web server. In other words, before making any adjustments it checks if the user has not changed the set point temperature. Then subroutine performs all sensors' readings. Based on this data and current mode it makes a decision whether it is reasonable to adjust the temperature in drying chamber. If the actual temperature in the drying chamber (T_1) is in the range $T_{sp} \pm tol$, where tol is a tolerance that allows deviations from the set point temperature, the program does not

perform any adjustments. However, if T_1 is out of this range subroutine calculates and assign new fan's speed (in Modes 1), new fan's speed and/or new heater's power (in Mode 2) or new heater's power (in Mode 3) according to the formulas in the flowchart.

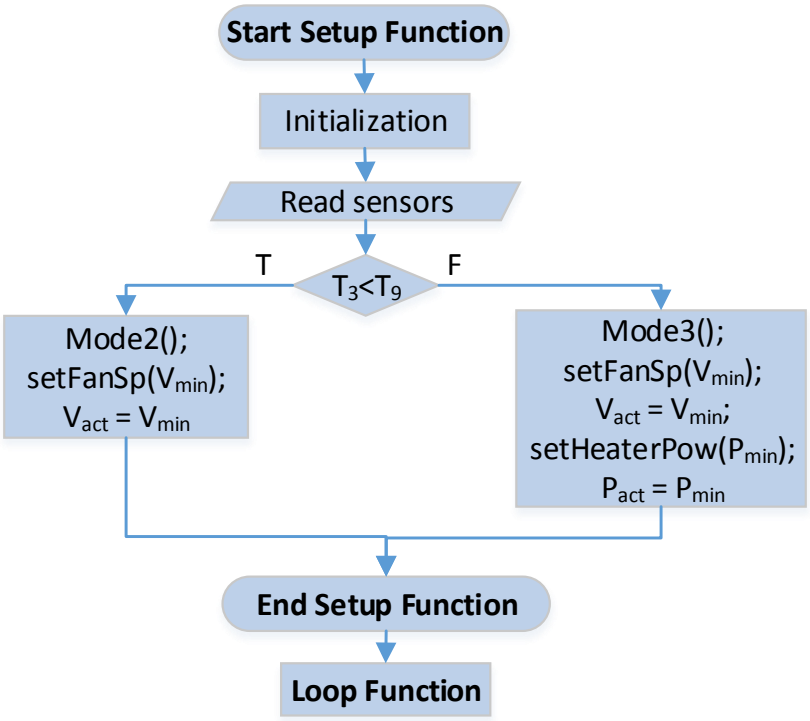

Figure 18. Flowchart of Setup Function:

V_{act} is actual fan speed, V_{min} is minimal fan speed, V_{max} is maximal fan speed, f is fan coefficient, *setFanSp()* is function that sets fan speed, P_{act} is actual heater power, P_{min} is minimal heater power, *setHeatPow()* is function that sets heater power, $T_{\#}$ - temperature reading by corresponding sensor

Since the software was implemented in C++ programming language that uses concepts of object oriented programming to give a glimpse of the software architecture it is reasonable to show messaging between different objects in the program. Figure 20 shows the interactions between the objects. Objects are presented in the boxes with their timelines as dashed lines. The first object is a user who sets the set point temperature on the web server. The EthernetClient object gets the set point temperature (T_{sp}) from the server and passes it to the main routing. The main routing reads all the sensors from the other objects: weight (from load cells amplifier HX711 object), temperature and humidity (from 1-Wire slave to I^2C master bridge device DS2482 object), tachometer value (from the Fan object), battery voltage (from Battery object).

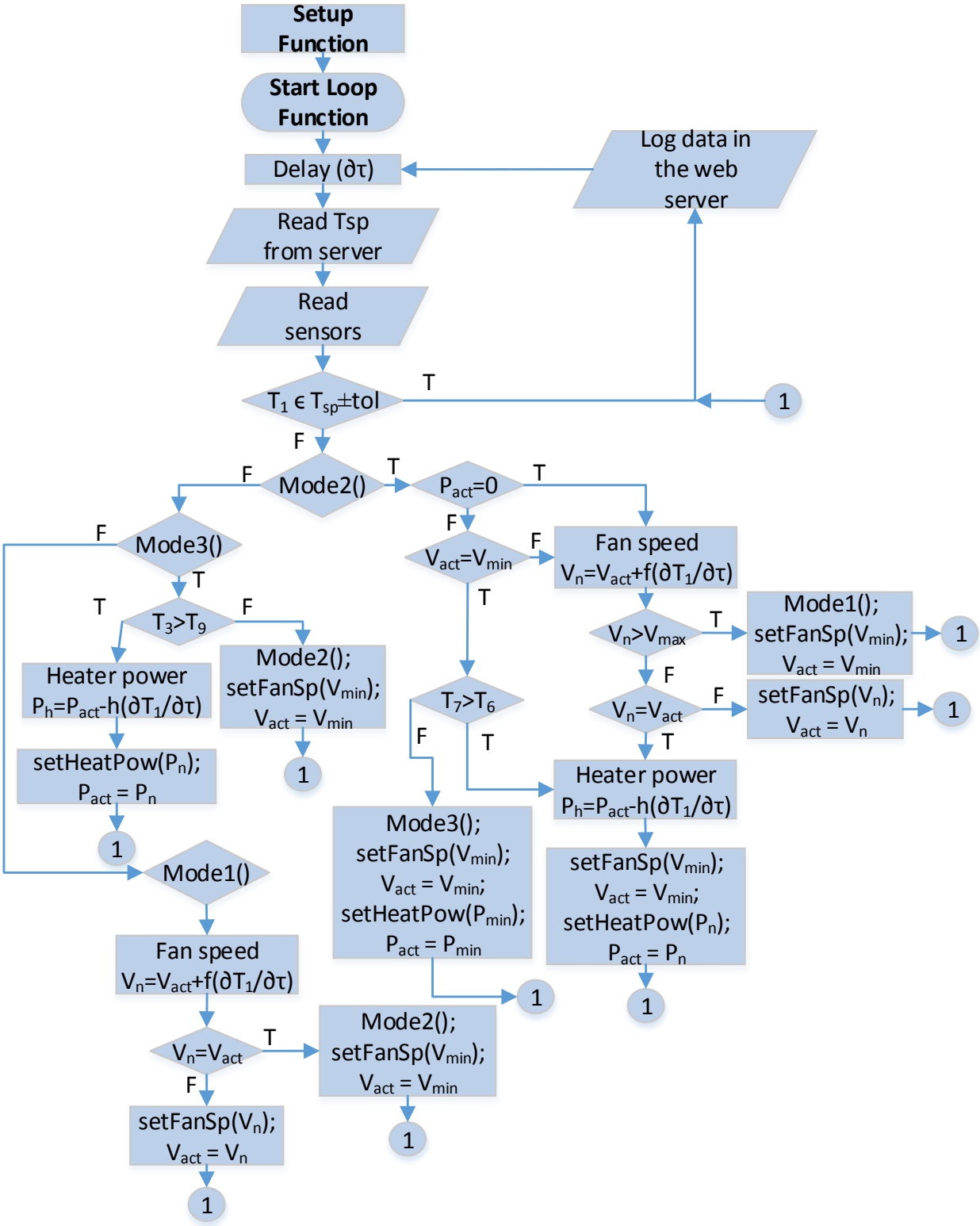

Figure 19. Flowchart of Loop Function:
$\partial T_1/\partial T$ is temperature change rate in the bottom of drying chamber, V_{act} is actual fan speed, V_n is new fan speed, V_{min} is minimal fan speed, V_{max} is maximal fan speed, f is fan coefficient, *setFanSp()* is function that sets fan speed, P_{act} is actual heater power, P_{min} is minimal heater power, P_{max} is maximal heater power, P_n is new heater power, h is heater coefficient, *setHeatPow()* is function that sets heater power, *tol* is tolerance that allows deviations from the set point temperature, $T_{\#}$ - temperature reading by corresponding sensor

After the main routing processed the collected data and defined mode, hater power and fan speed, it passes its decisions to the Mode object. The Mode object adjusts fan speed and heat power. Then the main routing passes sensors readings and decisions to the EthernetClient object that logs this data in the web server. A user could use data that are logged for further analysis.

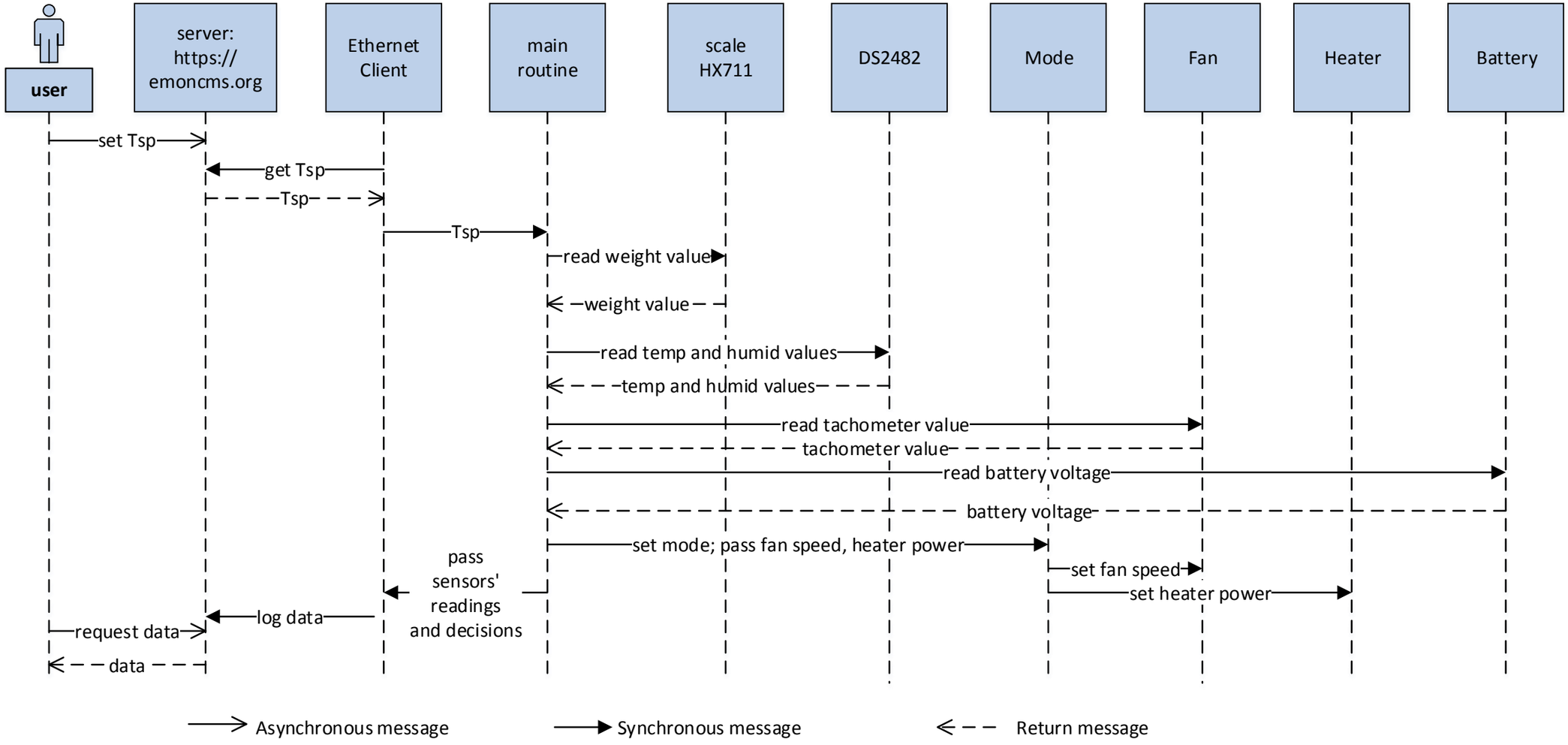

Figure 20. Object interaction diagram

4. Experimental

In order to measure irradiance to heat conversion ratio of the whole system working in Modes 1 and 2, we have performed experiments. They were performed indoors because we have finished the building of the setup in October and there was no solar irradiance available in Estonia. Five halogen lamps simulated the sunlight. The radiation level on the surface of PVT panels was measured by pyranometer and it was 235 W/m^2 in average. Air velocity measurements were performed using a hot wire anemometer.

The measurements of the temperature were conducted for different air velocities. Irradiance to heat conversion ratio for the Mode 1 and Mode 2 were calculated using equation (1) and (2) respectively.

$$R = \dot{m} \cdot c \cdot (T_7 - T_6)/(G \cdot A_c) \cdot 100 \quad (1)$$

$$R = \dot{m} \cdot c \cdot (T_3 - T_6)/(G \cdot A_c) \cdot 100 \quad (2)$$

where T_7, T_6 and T_3 are the temperatures of the air measured by the sensors 7, 6 and 3 shown on Figure 8 respectively, $\dot{m}$ is the mass flow rate of the air, c is specific heat capacity of the air, G is the radiation intensity on the collectors' surface measured by pyranometer and A_c is the area of the collectors.

5. Simulations

In order to perform the feasibility study, the system performance has been simulated under different climate conditions.

5.1. Thermal model of the air-type BIPVT collectors

For simulation of building integrated air-type photovoltaic-thermal collector, the model in the Ref. [20] was used. Figure 21 shows complex process of the heat transfer through the layers of PVT collector and the temperature nodes. Finite slab method was used for simulation of this process. The model takes into account solar irradiance, reflection from PV module, convective heat exchange between PV module, ambient air and the air in the channel, infrared heat exchange between the sky, ground, insulation layer and PV module. Authors simplified equations by assuming that temperatures of the cell, glass and back sheet over their cross section are uniform. When authors divided the structure on the slabs, they included half of encapsulant from each side of cells to the cells slab. This model allows the temperature change of the air over PV channel (z-axis).

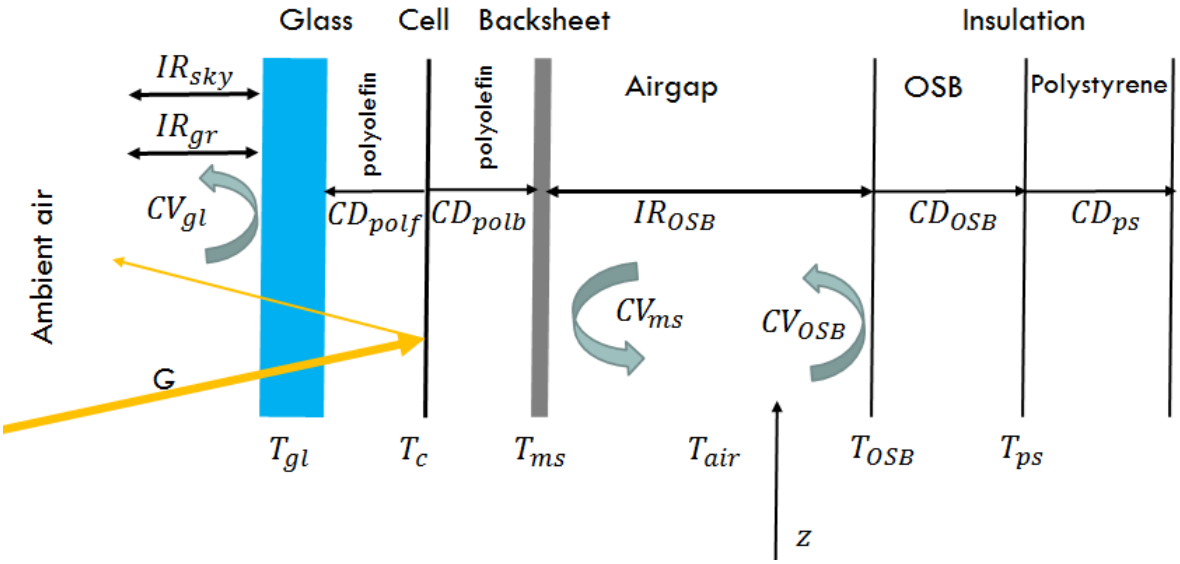

Figure 21. Heat transfer through the layers of BIPVT collector *[20]*

Solar irradiance absorption:

$$\alpha_{\mathrm{pv}} * \tau_{\mathrm{gl}} * G \tag{3}$$

where α_{pv} is PV cell absorption coefficient (0.97), τ_{gl} is glass transmittance (0.93), G is solar radiation intensity.

Infrared heat emitted from the glass to sky and ground:

$$IR_{gl} = \sigma * \epsilon_{gl} * T_{gl}^4 \tag{4}$$

where σ is Stefan-Boltzmann constant, ϵ_{gl} is glass emissivity (0.84), T_{gl} is glass temperature.

Infrared heat emitted from the sky to glass:

$$IR_{sky} = \sigma * VF_{sky} * T_{sky}^4 \tag{5}$$

where $T_{sky} = 0.05532 * T_{amb}^{1.5}$ is sky temperature, VF is view factor, T_{amb} is ambient air temperature.

Infrared heat emitted from the ground to glass:

$$IR_{gr} = \sigma * \epsilon_{gr} * VF_{gr} * T_{gr}^4 \tag{6}$$

where $\epsilon_{gr} = 0{,}8$ is ground emissivity, VF_{gr} is ground view factor, T_{gr} is ground temperature.

The metal sheet of the back of PV module has the exchange of the infrared radiation with the insulation layer through the air gap:

$$IR_{OSB} = \frac{\sigma * (T_{ms}^4 + T_{OSB}^4)}{1/\epsilon_{ms} + 1/\epsilon_{OSB} - 1} \tag{7}$$

where T_{ms}, T_{OSB} are absolute temperatures of the back metal sheet and oriented strand board surfaces, ϵ_{ms}, ϵ_{OSB} are emissivity of the back metal sheet and oriented strand board surfaces.

Heat conduction through each layer is defined by equation (heat flow direction showed on Figure 21):

$$CD = \frac{k(T_2 - T_1)}{x} \tag{8}$$

where k is thermal conductivity, x is slab thickness, T_2 is the temperature of the surface with higher temperature, T_1 is the temperature of the surface with lower temperature.

Convectional heat exchange of module and ambient air:

$$CV_{gl} = h_w * (T_{gl} - T_{amb}) \tag{9}$$

where T_{gl} is glass temperature, $h_w = 5.8 + 2.1 * ws$ is heat transfer coefficient and ws is wind speed.

Convectional heat exchange between air and channel walls is defined by equations:

$$CV_{ms} = hconv * (T_{ms} - T_{air}) \tag{10}$$

$$CV_{OSB} = hconv * (T_{OSB} - T_{air}) \tag{11}$$

where T_{air} is the temperature of the air inside the air gap, T_{ms} is module back metal sheet temperature, T_{OSB} is insulation surface temperature, $hconv$ is the heat exchange rate and defined by equation (12).

$$hconv = \frac{k_m}{D_h} * Nu \tag{12}$$

where k_m is thermal conductivity of air (dry air and water vapor mixture), $D_h = 4\frac{W*d}{2*(W+d)}$ is air channel hydraulic diameter, Nu is a Nusselt number (ratio of convective to conductive heat transfer) calculated according to Ref. [20].

The heat balances of each slab are defined by 6 differential equations (13)-(18) which are solved numerically in Mathematica.

1. Heat balance for the air gap:

$$\frac{\partial T_{air}}{\partial z} = \frac{hconv}{v_{air} d \rho_a c_a} (T_{ms} + T_{OSB} - 2T_{air}) \tag{13}$$

where v_{air} is the air flow speed, d is the thickness of the air channel, ρ_a is the density of the air in the channel, c_a is the specific heat of the air in the channel and z is the axis with the direction of the air flow and change in air temperature in the channel.

2. Heat balance for polystyrene layer:

$$\frac{m_{ps}c_{ps}}{2}\left(\frac{\partial T_{ps}}{\partial t}+\frac{\partial T_{in}}{\partial t}\right)=CD_{OSB}-CD_{ps} \tag{14}$$

where m_{ps}, c_{ps} are the mass and specific heat capacity of polystyrene and CD_{ps} is actually equal to CV_{ps} and T_{in} is temperature indoors.

3. Heat balance for the oriented strand board layer:

$$\frac{m_{OSB}c_{OSB}}{2}\left(\frac{\partial T_{OSB}}{\partial t}+\frac{\partial T_{ps}}{\partial t}\right)=-CD_{ps}+IR_{OSB}-CV_{OSB} \tag{15}$$

where m_{OSB}, m_{ps} are the mass of oriented strand board and polystyrene and c_{OSB}, c_{ps} are the specific heat capacity of oriented strand board and polystyrene.

4. Heat balance for the back metal sheet:

$$\left(m_{ms}c_{ms}+\frac{m_{polb}c_{pol}}{2}\right)\frac{\partial T_{ms}}{\partial t}=-IR_{OSB}+CD_{polb}-CV_{ms} \tag{16}$$

where m_{ms}, m_{polb} are the mass of metal sheet and polyolefin and c_{ms}, c_{pol} are specific heat capacity of metal sheet and polyolefin.

5. Heat balance for solar cell:

$$\left(m_{\mathrm{c}}c_{\mathrm{c}}+\frac{m_{polb}c_{pol}+m_{polf}c_{pol}}{2}\right)\frac{\partial T_{c}}{\partial t}=-CD_{polb}+\alpha_{pv}\tau_{gl}G-PV-CD_{polf} \tag{17}$$

where m_c is the mass of cells, c_c is specific heat capacity of cell and T_c – temperature of cell and PV is heat energy which is driven away by a current.

6. Heat balance for glass:

$$\left(m_{gl}c_{gl}+\frac{m_{polf}c_{pol}}{2}\right)\frac{\partial T_{gl}}{\partial t}=CD_{polf}+\alpha_{gl}G-CV_{gl}-IR_{gl}+IR_{sky}+IR_{gr} \tag{18}$$

where m_{gl} is the mass of glass, c_{gl} is the specific heat capacity of glass and α_{gl} is an absorption of the glass.

Initial conditions: $T_{i0}^{t=0}$=C1, $T_{i1}^{t=0}$=C2, $T_{bs}^{t=0}$=C3, $T_{air}^{t=0}$=C4, $T_{tc}^{t=0}$=C5, $T_{gl}^{t=0}$=C6.

5.2. The simulation of electricity production

In order to estimate production of electricity by PV panels, we simulated irradiance on tilted surface based on global horizontal and diffused irradiance using Perez model from the Ref. [21].

The temperature of the modules was calculated by equation *(17)* from the thermal model of BIPVT collectors.

Module output power:

$$P_{mod} = P_{max}\, G'(1 + C_0 log G' + C_1 log G' + \gamma T') \tag{19}$$

where P_{max} is maximum power of the module under standard test conditions taken from the datasheet, γ is the temperature coefficient of maximum power taken from the datasheet, $G' = G/1000$, $T' = T_{mod} - 25$ (where T_{mod} is the temperature of the modules) and $C_0 = -0{,}01228$, $C_1 = -0{,}01681$ are coefficients for crystalline silicon cells.

5.3. The simulation of the HRU

The measurements of the air temperatures during the experiments gave an opportunity to calculate the efficiency of the HRU at the different air flow rates. The efficiencies of the HRU were calculated using the equation (20) and presented on Figure 22.

$$\eta_{HRU} = (t_4 - t_3) / (t_5 - t_3) \tag{20}$$

where η_{HRU} is calculated efficiency of the HRU based on measured data, t_3, t_4 and t_5 are the temperatures of the air measured by the sensors 3, 4 and 5 shown on Figure 8 respectively.

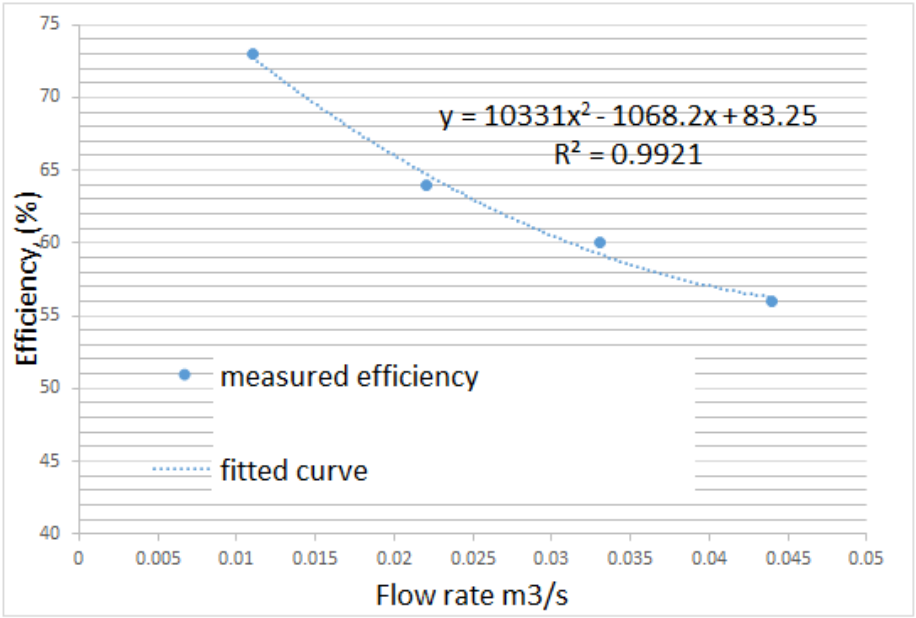

Figure 22. Efficiency versus air flow rate

Polynomial equation (21) was fitted to the experimental data in order to conduct the simulations.

$$\eta_{HRUtheor} = 10331 \cdot \dot{m}^2 - 1068.2 \cdot \dot{m} + 83.25 \quad (21)$$

where $\eta_{HRUtheor}$ is calculated efficiency of the HRU based on the fitted equation, $\dot{m}$ is an air mass flow rate.

5.4. The simulation of the heater

The heat power transferred from the heater to the air:

$$P_h = I_h U_h = c_a \dot{m} \Delta T \quad (22)$$

where I_h is the current consumed by the heater, U_h is voltage, ΔT is the difference between the temperature of the air after and before the heater and c_a is the specific heat of the air.

5.5. The simulation of the batteries

The surplus electrical power from the charge controller to the batteries and from the batteries to system's elements was calculated:

$$E_b(i) = E_b(i-1) + \eta\, I_{inb} U_b - I_{outb} U_b \tag{23}$$

where $E_b(i)$ is the level of energy in batteries during the current hour, $E_b(i-1)$ is the level of energy in batteries during the previous hour, I_{inb} is current into batteries, I_{outb} is current out from batteries, U_b = 24 V is batteries voltage, $\eta = 0{,}8$ – efficiency

5.6. Estimation of the fan consumption

In order to estimate the fan consumption we used following method. The average air flow rate in the simulations was 0.05 m^3/s. Experimentally, we measured the electrical power of the fan when it worked with the air flow rate of 0.05 m^3/s**.** Measured power was 67W.

Fan consumption during simulated period was calculated by equation:

$$E_f = P_f t \tag{24}$$

where P_f is the measured power and t = 2930h is time.

6. Results and discussion

From the indoor experiments, we have obtained an irradiance to heat conversion ratio in Modes 1 and 2. It is the ratio between heat power produced by the system to solar irradiance power on the top of the roof.

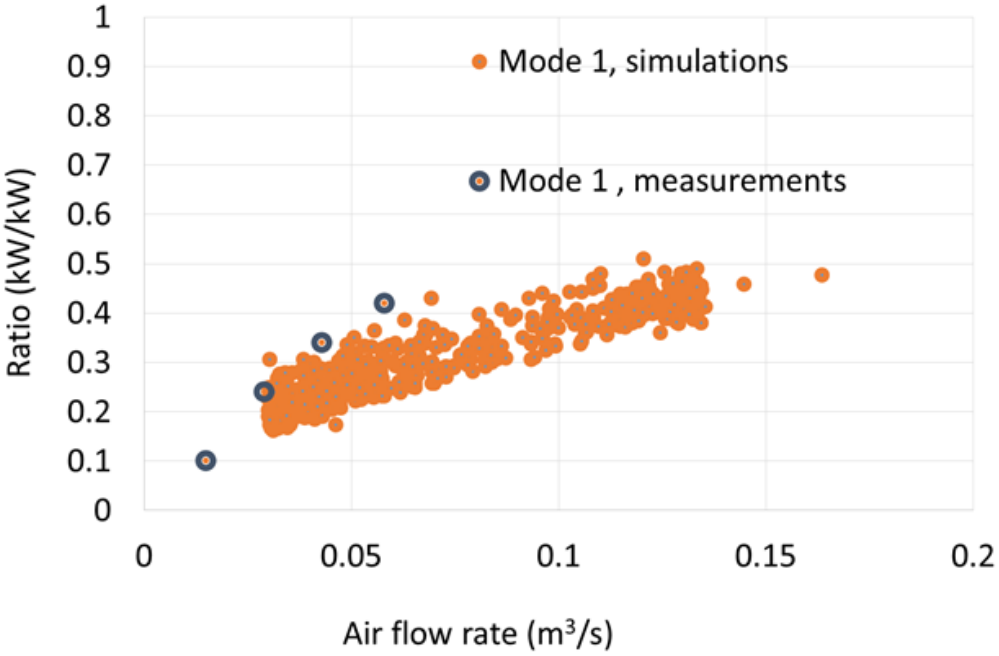

Figure 23. Irradiance to heat conversion ratio of the Mode 1

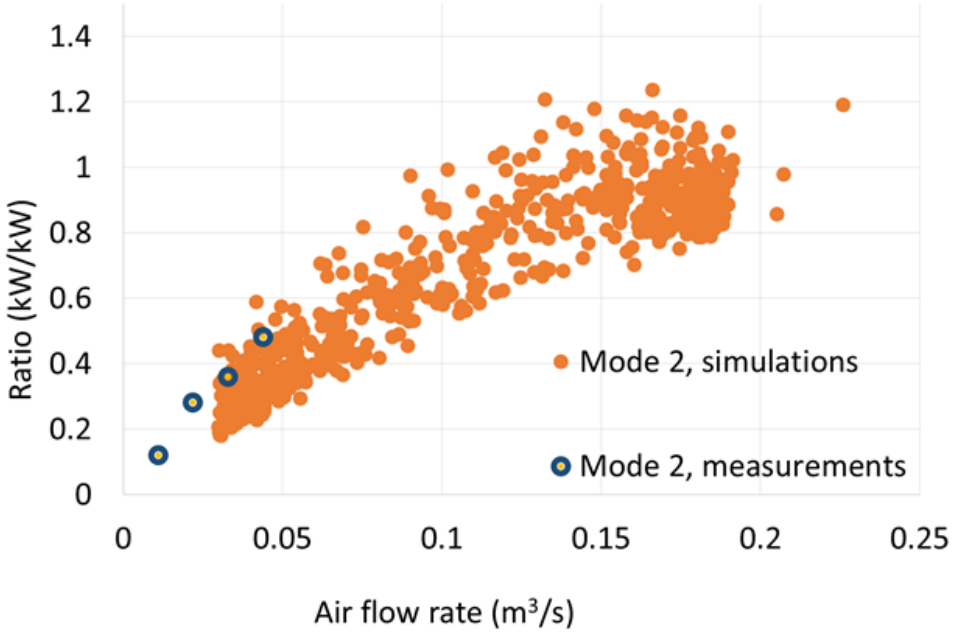

Figure 24. Irradiance to heat conversion ratio of the Mode 2

Experimentally we have achieved an irradiance to heat conversion ratio about 0,4 kW/kW and 0,5 kW/kW with air flow rate about 0,05 m^3/s in Modes 1 and 2 respectively. We could not test the system with higher flow rates because we have chosen the fan with too low power. However, the results of simulations for summer period in Estonia show that it is possible to achieve an irradiance to heat conversion ratio of 0,5 kW/kW with air flow rate of 0,13 m^3/s and 1,2 kW/kW with air flow rate of 0,15 m^3/s in Modes 1 and 2 respectively. Experimental data on Figure 23 and Figure 24 are higher than simulated and there is the significant reason. Simulations were conducted for outdoors conditions whereas experimental results were obtained from indoors experiments. There are much less infrared and convectional losses indoors. The high ratio in Mode 2 is explained by the fact that part of the heat is recovered by HRU. Irradiance to heat conversion ratio depends on the air flow rate and increases with the air flow rate increase. This is because of the thermal losses on top of the roof to the ambient air. They are reduced when the BIPV modules are cooler. However, the system cannot always run with the maximum irradiance to heat conversion ratio because the air flow rate is mostly determined by the set point temperature in the drying chamber. In the case of too high flow rates, the BIPV modules are cooled below the desired temperature. Therefore, it is impossible to achieve set point temperature in the drying chamber.

Table 2 shows key results of the simulations of the drying system's performance during the season June – September (2928 hours) in Tallinn and Provence.

Table 2. Key indicators of system's performance simulations for different locations

Location	Estonia, Tallinn	France, Provence
Total collected solar energy by the roof (kWh)	4049	5579
Electrical energy from PV (kWh)	457	621
Total produced heat energy (kWh)	3223	3479
Fan consumption (kWh)	196	196
Electricity from batteries (kWh)	180	236
Auxiliary electrical energy, for 24/7 operation (kWh)	355	142
Autonomous hours, when auxiliary power = 0 (h)	1494	2193
Maximum PV power (kW)	0.8	0.8
Maximum heater power (kW)	1.1	1.0
Maximum charge power (kW)	0.8	0.8
Batteries' capacity (kWh)	5.8	5.4

Total produced heat energy in Table 2 is heat energy produced by the system including heat from BIPVT collectors and electrical heater that uses electricity from PV panels, batteries and auxiliary electrical source. The system receives by 37% more solar irradiance and produces only by 8% more heat energy in Provence comparing to Tallinn. Despite the fact that the system does not produce the significantly larger amount of heat energy in Provence, it runs 76% of time autonomously in contrast with 51% in Tallinn.

Table 2 also shows that for 24/7 operation the system still requires the additional electrical energy of 355 kWh and 142 kWh in a season in Tallinn and Provence respectively. Figure 25 presents the correlation between the backup power and solar irradiance. The system does not need auxiliary electrical power when the solar radiation is higher than 300 W/m^2 and 400 W/m^2 in Tallinn and Provence respectively. Such a difference between required powers for different locations is explained by a difference in ambient temperatures.

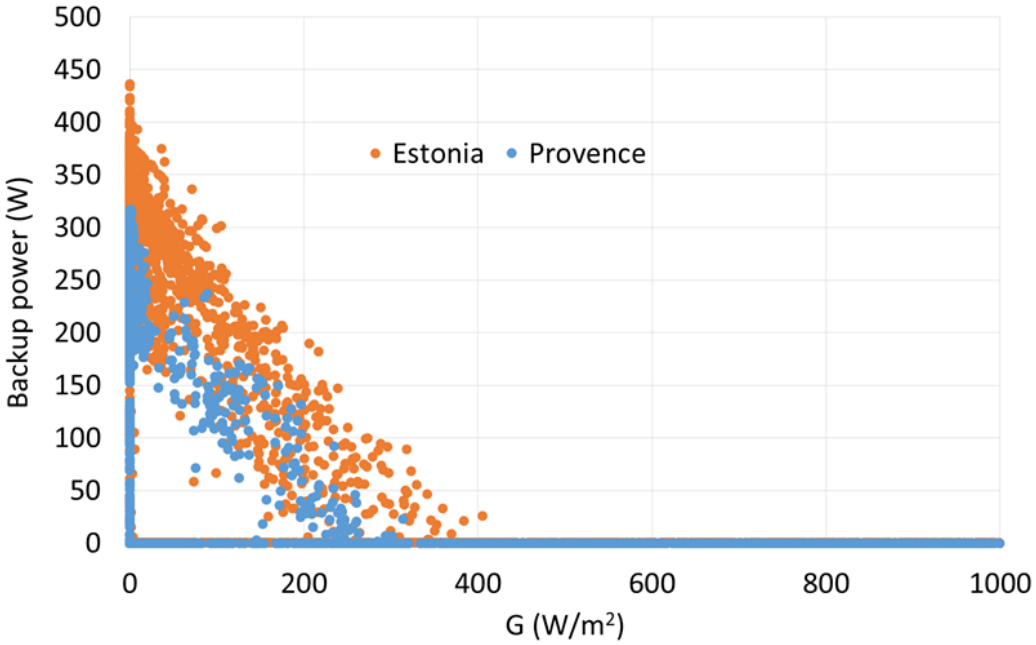

Figure 25. Required auxiliary electrical power

The system can run in three operational modes and Figure 26 shows the shares of hours in different modes in Tallinn and Provence in a season. In Provence system can run much more time in modes 1 and 2, that affects the energetic autonomy of the system positively. Because less electrical energy is required for heating.

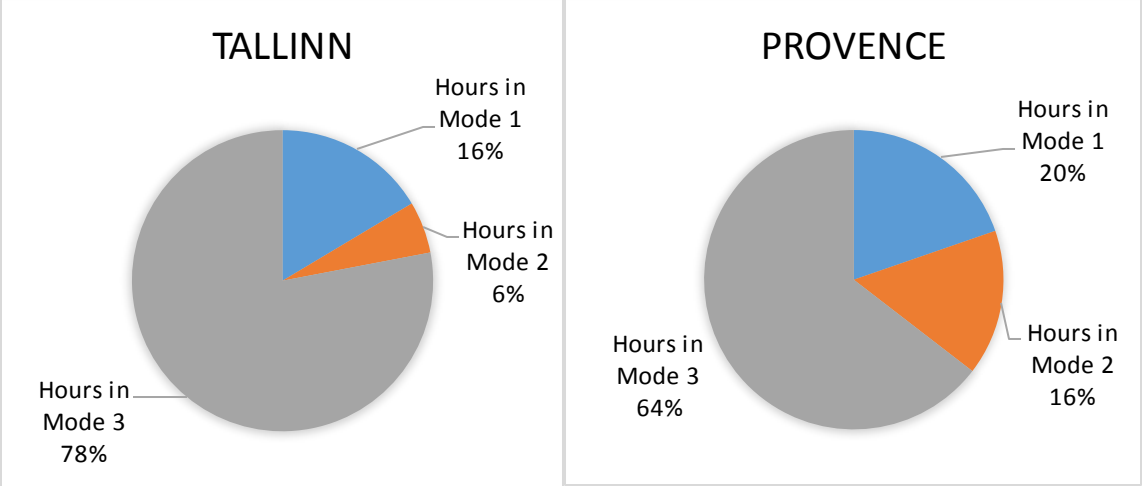

Figure 26. Shares of hours working in different modes

Results of simulations showed that we need at least to double batteries' electrical capacity and the heater power. We have chosen the heater that is made out of aluminum. The resistance of such heaters drops down significantly with temperature rise. The actual current for heating was at least two times higher than expected. Therefore, the heater should be replaced.

We designed drying chamber only for one-directional air flow through the products. This approach has the significant disadvantage. The drying rate of all the trays would be different all the time. In order to equalize the drying rate of product on all the trays, it is more convenient to use bidirectional air flow. Therefore, the products on all trays would be dried at the same time. It is reasonable to rebuild the system with the possibility of bidirectional air flow through the drying chamber. However, such a system would be more complex and expensive.

7. Conclusions

The test bench of indirect solar drying system has been developed, built and tested indoors. We have developed and presented the structure of BIPVT collectors, electronic circuits to control separate parts of the system, three operational modes and possible working algorithm.

Experimentally we achieved irradiance to heat conversion ratio of such a system of 0.4 kW/kW in Mode 1 and 0.5 kW/kW in Mode 2. Simulated data show that it is possible to have heat conversion ratio between 0.3 – 1.2 kW/kW depending on air flow rate and operational mode. The use of HRU in Mode 2 is justified and increases the heat conversion ratio as it recovers part of the heat energy. With the same air flow rate as in Mode 1, it is possible to achieve higher irradiance to heat conversion ratio.

The system can produce 3223 kWh of heat energy in Tallinn and 3479 kWh in Provence in a season. For 24/7 operation the system needs extra electricity in Tallinn 355 kWh and in Provence 142 kWh. The system can run autonomously for 76% and 51% of the time in a season in Provence and Tallinn respectively.

For irradiance level higher than 300 W/m^2 in Provence and 400 W/m^2 in Tallinn system is fully autonomous. The difference in irradiance is explained by the difference in ambient temperatures.

Indirect solar drying with BIPVT collectors is a competitive technology with industrial food dehydrators. The price level for such drying system is about the same as industrial electrical dryers with the power of 1 kW. The amount of energy produced by the systems in a season is approximately same.

Plans for future are to increase the fan’s power, heater’s power and batteries' electrical capacity, to rebuild system piping in order to provide bidirectional air flow through the drying chamber, to perform outdoor experiments under loaded conditions.

Résumé

This study aims to share experience in designing, building and testing of the portable and energetically autonomous food dehydration system based on the air type BIPVT roof and to perform simulations of drying system performance under different climate conditions (Tallinn, Estonia and Provence, France) in order to estimate the feasibility of this technology.

The drying system is based on air-type BIPVT collectors as main heat and electricity source. BIPVT collectors are metal sheet integrated PV modules with the air gap organized under PV modules. The total area of the roof is 7m^2. The total power of PV panels is 1kW. In addition, the system comprises the piping system, fan, batteries, dampers, HRU, drying chamber and the electrical heater for auxiliary heating. The system can work in three operational modes depending on weather conditions. The modes are defined by the dampers positions that allow to regulate the air movement through the system's elements. The first mode is designed for periods with the most intensive solar radiation when the production of heat from BIPVT is high enough to provide suitable temperature regime in drying chamber. Therefore, the air is heated only by collectors, directed to the drying chamber and released to the environment. The temperature in the drying chamber is regulated by the fan speed in Mode 1. Mode 2 is designed for periods with low-level solar irradiance when there is some production of heat from BIPVT collectors but it is not high enough to achieve needed temperature in the drying chamber. In this case, the air is taken from the outside, preheated in the HRU, if the temperature is not high enough than it is heated by the electrical heater, directed to the drying chamber, heated by BIPVT collectors and released to the environment through the HRU. The temperature in the drying chamber is regulated by both the fan speed and the heating power. Mode 3 is designed for night periods or periods when solar energy is unavailable. In this case, the air is heated by the electrical heater and also part of the heat is recovered by the HRU. The system uses the minimum fan speed and the temperature is regulated by the heating power.

During indoor experiments, we have obtained irradiance to heat conversion ratio that is the ratio of irradiance power solar on top of the roof to heating power produced by the system. It was about 0.4 kW/kW in Mode 1 and 0.5 kW/kW in Mode 2. However, the results of the simulations showed that it is possible to achieve irradiance to heat conversion ratio between 0.3 – 1.2 kW/kW depending on air flow rate and operational mode. The results of the simulations during period June – September under Estonian conditions showed that total produced heat energy by the system is 3223 and 3479 kWh in Tallinn and Provence respectively. However, for autonomous operation for 24/7 during June – September the system requires additional electricity of 355 and 142 kWh in Tallinn and Provence respectively. When irradiance level is higher than 300 W/m^2 in Provence and 400 W/m^2 in Tallinn the system is fully autonomous.

Resümee

Töö eesmärgiks on ehitisintegreeritud päikesepaneelide baasil loodud autonoomse toiduainete kuivati prototüübi projekteerimine, ehitamine, testimine ning modelleerimine. Kuivati energiaallikaks on ehitisintegreeritud päikesepaneelid, mida kasutatakse elektri ning soojuse koostootmiseks. Kuivati tööks vajalikku sooja õhku saadakse päikesepaneelide all olevast kitsast õhukanalist. Prototüübi päikesepaneelide pindala on 7 m^2 ning nominaalne võimsus 1 kW. Lisaks päikesepaneelidele on süsteemi peamisteks komponentideks veel ventilatsioonitorustik, ventilaator, akud, ventilatsiooniklapid, soojustagasti, kuivatuskamber ning elektriline küttekeha.

Vastavalt kiirgushulgale saab klappide abil reguleerida süsteemi töörežiimi. Süsteem töötab esimeses režiimis kui päikesekiirguse hulk on piisav, et kütta päikesepaneelide all olevast kanalist väljuv õhk kuivatamiseks sobilikule temperatuurile. Esimeses režiimis võetakse õhukanalisse sisenev õhk otse väliskeskkonnast. Kuivatuskambrisse siseneva õhu temperatuuri saab reguleerida muutes ventilaatori kiirust. Teine töörežiim on mõeldud kasutamiseks keskmise päikesekiirguse intensiivsuse korral. Sellisel juhul kasutatakse külma välisõhu eelsoojendamiseks süsteemist väljuvat kuuma õhku. Lisakütte allikana saab kasutada teises režiimis elektrilist küttekeha. Kolmas režiim on mõeldud kasutamiseks öösel. Sellisel juhul toimub kuivatusõhu soojendamine ainult süsteemist väljuva õhu ning elektrilise küttekeha arvel. Kolmandas režiimis töötab ventilaator minimaalsel kiirusel ning kuivatusõhu temperatuuri reguleerimine toimub elektrilise küttekeha võimsuse kaudu.

Magistritöö käigus katsetasime kuivati prototüüpi sisetingimustes kunstliku valgusallika all. Katsete tulemused näitasid, et esimeses režiimis on võimalik saavutada kiirguse konverteerimine kasulikuks soojusenergiaks suhtega 0.4 kW/kW. Teises režiimis saime tulemuseks suhte 0.5 kW/kW. Simulatsioonide tulemused aga näitasid, et teoreetiliselt peaks olema võimalik saavutada vastav suhe sõltuvalt õhu vooluhulgast vahemikus 0.3 – 1.2 kW/kW. Katsete ning simulatsioonide omavahelised võrdlused näitasid, et parema suhtarvu saavutamiseks peaksime suurendama prototüübi ventilaatori võimsust.

Pikema perioodi simulatsioonide tulemused erinevate geograafiliste piirkondade kohta näitasid, et juunist kuni septembrini on prototüübi toodetud soojusenergia Eestis 3223 kWh ja Provence'is (Lõuna-Prantsusmaal) 3479 kWh. Süsteemi töötamiseks 24/7 jääb Eestis puudu 355 kWh ning Provence'is puudu 142 kWh elektrienergiat. Alates päikesekiirguse intensiivsustest 300 W/m^2 Provence'is ning 400 W/m^2 Eestis on portotüüp täisautonoomne.

References

[1] V. Belessiotis and E. Delyannis, "Solar drying," *Solar Energy,* no. 85, p. 1665–1691, 2011.

[2] S. Hendrie, "Photovoltaic/thermal Collector Development Program—Final Report," Lincoln laboratory, Lexington, 1982.

[3] T. Russell, J. Beall, J. Loferski, B. Roessler, R. Dobbins, J. Shewchun, J. Krikorian, C. Case, G. Doodlesack and W. Oates, "Combined photovoltaic/thermal collector panels of improved design," in *IEEE Photovoltaic Specialists Conference*, Washington, DC, 1981.

[4] T. Bergene and O. Løvvik, "Model calculations on a flat-plate solar heat collector with integrated solar cells," *Solar Energy,* no. 55 (6), p. 453–462, 1995.

[5] Y. T ripanagnostopoulos, T. Nousia and . P. Yianoulis, "Hybrid photovoltaic/thermal solar systems," *Solar Energy,* no. 72 (3), pp. 217-234, 2002.

[6] G. Rockendorf, R. Sillman, L. Podlowski and B. Litzenburger, "PV-hybrid and thermo-electric-collectors," in *ISES 1999 Solar World Congress*, Jerusalem, 1999.

[7] R. Kumar and M. A. Rosen, "A critical review of photovoltaic–thermal solar collectors for air heating," *Applied Energy,* no. 88, p. 3603–3614, 2011.

[8] A. Kumar, P. Baredar and U. Qureshi, "Historical and recent development of photovoltaic thermal (PVT) technologies," *Renewable and Sustainable Energy Reviews,* no. 42, p. 1428–1436, 2015.

[9] A. A. Hegazy, "Comparative study of the performances of four photovoltaic/thermal solar air collectors," *Energy Conversion & Management* , no. 41, pp. 861-881, 2000.

[10] S. Solanki, S. Dubey and A. Tiwari, "Indoor simulation and testing of photovoltaic thermal (PV/T) air collectors," *Applied Energy,* no. 86, p. 2421–2428, 2009.

[11] B. Agrawal and G. Tiwari, "Life cycle cost assessment of building integrated photovoltaic thermal (BIPVT) systems," *Energy and Buildings,* no. 42, p. 1472–1481, 2010.

[12] A. Fudholi , K. Sopian, M. Ruslan, M. Alghoul and M. Sulaiman, "Review of solar dryers for agricultural and marine products," *Renewable and Sustainable Energy Reviews,* no. 14, pp. 1-30, 2010.

[13] M. Ruslan, M. Othman, B. Yatim, K. Sopian, M. Ali and Z. Ibrahim, "Photovoltaic assisted solar drying system," *Proceeding of the International Symposium*, p. 681–687, 2003.

[14] A. Pratoto, M. Daguenet and B. Zeghmati, "Sizing solar assisted natural rubber dryers," *Solar Energy*, p. 287–291, 1997.

[15] A. J. N. Khalifa, A. M. Al-Dabagh and W. M. Al-Mehemdi, "An Experimental Study of Vegetable Solar Drying Systems with and without Auxiliary Heat," *ISRN Renewable Energy*, 2012.

[16] M. Othman, B. Yatim, K. Sopian, A. Zaharim and M. Bakar, "Studies of A Photovoltaic-Thermal Solar Drying System For Rural Applications," *International Conference on RENEWABLE ENERGY SOURCES*, pp. 132-136, 2008.

[17] M. Slimani, M. Amirat, S. Bahria, I. Kurucz , M. Aouli and R. Sellami, "Study and modeling of energy performance of a hybrid photovoltaic/thermal solar collector: Configuration suitable for an indirect solar dryer," *Energy Conversion and Management*, no. 125, p. 209–221, 2016.

[18] I. McDoom, R. Ramsaroop, R. Saunders and A. Tang Kai, "Optimization of solar crop drying," *Renewable Energy*, no. 16, pp. 749-752, 1999.

[19] M. Aktas, S. Sevik, A. Amini and A. Khanlari, "Analysis of drying of melon in a solar-heat recovery assisted infrared," *Solar Energy* , no. 137, p. 500–515, 2016.

[20] A. Jagomägi, "Thermal model of building integrated air type photovoltaic-thermal system under varying conditions," *32nd European Photovoltaic Solar Energy Conference and Exhibition*, pp. 2740 - 2745, 2016.

[21] R. Perez, R. Seals, P. Ineichen, R. Stewart and D. Menicucci, "A new simplified version of the Perez diffuse irradiance model for tilted surfaces," *Solar Energy*, vol. 39, no. 3, pp. 221-231, 1987.

[22] F. Olmo, J. Vida, I. Foyo, Y. Castro-Diez and L. Alados-Arboledas, "Prediction of global irradiance on inclined surfaces from," *Energy* , no. 24, p. 689–704, 1999.

Appendix 1

Acknowledgements

I would like to express my deep gratitude to my supervisor Dr. Andri Jagomägi for his professional guidance, valuable support, assistance, advices and time that he spend. It would be just impossible to accomplish this study without him.

I send special thanks to the Dean of Faculty of Chemical and Material Technology, and the Head of Department.

This work was supported by institutional research funding IUT (IUT19-28) of the Estonian Ministry of Education and Research, by the European Union through the European Regional Development Fund project TK141. The research has been done in collaboration with the private company ROOFIT SOLAR ENERGY OÜ.

Finally, special recognition goes out to my family for their support and encouragement.

Appendix 2

This work was presented at the PhotoVoltaic Technical Conference 2017 (the 8th event of a series of international PV specialty conferences) with an oral presentation entitled: "Development of autonomous food dehydration system based on building integrated PVT technology", at the International Center of Villa Méditerranée, Marseille, France.